AGU PUBLICATIONS

JGR

Journal of Geophysical Research: Oceans

RESEARCH ARTICLE

10.1002/2014JC010440

Wave power variability and trends across the North Atlantic influenced by decadal climate patterns

Peter D. Bromirski[1] and Daniel R. Cayan[2]

[1]Scripps Institution of Oceanography, UCSD, La Jolla, California, USA, [2]Scripps Institution of Oceanography and U.S. Geological Survey, La Jolla, California, USA

Key Points:
- Wave power variability over the North Atlantic is strongly influenced by the phase of the NAO
- Long-term upward trends in wave power strongly depend on record length and epoch
- Western boundary wave activity is influenced by North Pacific climate patterns

Supporting Information:
- Basin-wide Spatial Patterns and Temporal Variability
- Readme
- Wave Model Performance Validation

Correspondence to:
P. D. Bromirski,
pbromirski@ucsd.edu

Citation:
Bromirski, P. D., and D. R. Cayan (2015), Wave power variability and trends across the North Atlantic influenced by decadal climate patterns, *J. Geophys. Res. Oceans*, *120*, 3419–3443, doi:10.1002/2014JC010440.

Received 9 SEP 2014
Accepted 12 APR 2015
Accepted article online 24 APR 2015
Published online 9 MAY 2015

Abstract Climate variations influence North Atlantic winter storm intensity and resultant variations in wave energy levels. A 60 year hindcast allows investigation of the influence of decadal climate variability on long-term trends of North Atlantic wave power, P_W, spanning the 1948–2008 epoch. P_W variations over much of the eastern North Atlantic are strongly influenced by the fluctuating North Atlantic Oscillation (NAO) atmospheric circulation pattern, consistent with previous studies of significant wave height, *Hs*. Wave activity in the western Atlantic also responds to fluctuations in Pacific climate modes, including the Pacific North American (PNA) pattern and the El Niño/Southern Oscillation. The magnitude of upward long-term trends during winter over the northeast Atlantic is strongly influenced by heightened storm activity under the extreme positive phase of winter NAO in the early 1990s. In contrast, P_W along the United States East Coast shows no increasing trend, with wave activity there most closely associated with the PNA. Strong wave power "events" exhibit significant upward trends along the Atlantic coasts of Iceland and Europe during winter months. Importantly, in opposition to the long-term increase of P_W, a recent general decrease in P_W across the North Atlantic from 2000 to 2008 occurred. The 2000–2008 decrease was associated with a general shift of winter NAO to its negative phase, underscoring the control exerted by fluctuating North Atlantic atmospheric circulation on P_W trends.

1. Introduction

Populated coastal zones of the North Atlantic are vulnerable to winter storm wave impacts. The greatest societal impacts result when high waves occur near high tide, producing coastal flooding as well as beach erosion, affecting coastal infrastructure and the economies of coastal communities. Strong wave events that regularly impact the U.S. East Coast and the Atlantic coast of Europe during winter have cumulative coastal erosion effects, as well as significant economic and environmental impacts [*Mather et al*., 1967; *Dolan et al*., 1988; *Dolan and Davis*, 1992]. Increases in winter wave power and their characteristics along coasts are thus important considerations for mitigation and adaptation planning in response to sea level rise. Because extreme waves generally coincide with extreme surge [*Cayan et al*., 2008] and extreme rainfall [*Bromirski and Flick*, 2008], intensified storminess in the northeast Atlantic can have significant impacts not only along coasts, but farther inland as well. In contrast to negative effects from fossil fuel emissions, increasing wave power, P_W, could provide an important renewable and sustainable energy resource that does not have negative environmental impacts [*Clément et al*., 2002].

In the western North Atlantic, an early version of the temporal climatology of eastern U.S. coastal storms was described by *Mather et al*. [1964] and then further developed by *Dolan et al*. [1988] and *Davis et al*. [1993], both of whom used wave heights as a criterion for describing the synoptic storm climatology. These latter two analyses used wave height hindcasts that ended in 1984, concluding that the most damaging storms occurred during winter months. More recently, *Hirsch et al*. [2001] described the East Coast winter storm climatology using NCEP-NCAR reanalysis sea level pressure and wind data sets from 1951 to 1997, finding no significant trends in storm frequency.

In the northeast Atlantic, an intensification of the wave climate has been observed during the 1970s and 1980s [*Carter and Draper*, 1988; *Bacon and Carter*, 1991, 1993; *Bouws et al*., 1996; *WASA Group*, 1995], and inferred from modeled hindcasts by several studies over various time periods, generally finding upward trends in significant wave height, *Hs*, over the northeast Atlantic during the latter half of the twentieth

century (e.g., *Kushnir et al*. [1997], 1980–1989; *Wang and Swail* [2001], 1955–1994; *Cox and Swail* [2001], 1958–1997; *Wang et al*. [2006], 1958–2001; *Semedo et al*. [2011], 1957–2002; *Dodet et al*. [2010], 1953–2009, focused on the northeast Atlantic) and in the Bay of Biscay (1958–2001) [*Charles et al*., 2012]. These studies found that wave and storm variability are linked to changes in broad-scale climate patterns, with wave intensification associated with the positive phase of the North Atlantic Oscillation (NAO) [*Barnston and Livezey*, 1987; *Hurrell*, 1995; *Cassou et al*., 2004; *Hurrell et al*., 2003]. Affecting storm track location, the NAO alternates between the stronger midlatitude westerly wind (positive) phase associated with a deep Icelandic low, strong Azores high pressure cells, and the weaker westerly wind (negative) phase associated with the weaker form of these centers of action. Fluctuations in the NAO occur over a range of frequencies [*Hurrell and van Loon*, 1997] and are known to have a significant effect on wave intensity and distribution over the North Atlantic [*Bacon and Carter*, 1993; *Kushnir et al*., 1997; *Cox and Swail*, 2001]. Here we employ a several decade simulation of wind waves in the North Atlantic to investigate how decadal variability of the NAO has affected variability and long-term trends of *Hs*, wave power, and high wave events.

As climate changes, there may be changes in storm track and intensity over midlatitude ocean basins [*IPCC*, 2013], which could produce changes in wave climate. However, identifying reliable trends in regional wave activity from relatively short duration buoy records in the presence of potentially significant climate-related decadal variability, such as along the U.S. East Coast, is a challenge because they are sparse point-measurements [*Bidlot et al*., 2002], many of which are likely contaminated by instrumental problems [*Gemmrich et al*., 2011]. Many of the drawbacks associated with buoy records in identifying broad-scale spatial patterns of wave activity over a range of time scales from synoptic to multidecadal, including trends, can be overcome using wave model hindcasts, which have been shown to have reasonably good agreement with reanalyzes and buoy measurements [*Cox and Swail*, 2001; *Graham and Diaz*, 2001; *Caires et al*., 2004, *Semedo et al*., 2011; *Bromirski et al*., 2013].

Because storm impacts on coastal processes depend in part on the rate at which wave energy is delivered, wave power is a better descriptor of storm strength than *Hs* alone. Wave power variability in the western North Atlantic has been associated with hurricane intensity in the basin [*Bromirski and Kossin*, 2008], and with broad-scale climate variability over the North Pacific [*Bromirski et al*., 2013]. Accordingly, in addition to *Hs*, which has been the main focus of most previous investigations, this study investigates wave power, including spatial patterns, multiyear variability, trends, and related characteristics of extreme high wave events. We follow the analysis methodology presented in *Bromirski et al*. [2013] for the North Pacific, but here focusing on western and northeastern North Atlantic wave activity. The wind-forced wave model data examined in the present study spans 1948–2008, a period that is longer than was available in most previous studies, which affords a better sample of interannual and especially decadal variability.

The paper is structured as follows. First, the data and analysis methods are described, with discussion of comparisons between wave model *Hs* and buoy *Hs* to validate the model data. Then the spatial distributions of *Hs*, *Tp*, and P_W over the North Atlantic during both winter and summer seasons are described, establishing trends of both the long-term mean and heightened levels of these wave characteristics. Their spatial distribution is described using empirical orthogonal functions, and the associations with well-known patterns of climate variability are determined from correlations of the associated principal components. Next, two different designations of wave events, those exceeding the ninetieth percentile *Hs* threshold and those most extreme winter and summer events of each year, are investigated, including a description of their spatial distribution, duration, associated P_W, and their trends. Finally, regional and eastern North Atlantic wave power variability and its relationship to broad-scale climate patterns are explored.

2. Data and Methods

2.1. Wave Model Data

A global hindcast of ocean gravity wave heights spanning the 1948–2008 time period was generated with the WAVEWATCH III ver 3.14 (WW3) [*Tolman*, 2009] wave model. The WW3 wave model was run over a 1.0° × 1.0° latitude and longitude resolution global domain forced by NOAA National Centers for Environmental Prediction (NCEP) reanalysis project [*Kalnay et al*., 1996] global near-surface winds (NRA-1), described in detail in *Bromirski et al*. [2013]. Ice concentration below 33% is considered open ocean, and above 67% is treated as land. Between these bounds, the swell is attenuated by the percentage of ice concentration. This

study focuses on the North Atlantic subset of the global WW3 model significant wave height, *Hs*, and peak wave period, *Tp*, outputs, although waves generated south of the North Atlantic analysis domain are necessarily included in the analyses.

2.2. Analysis Methodologies

In this study, the following measures of wave variability and changes within the six-decade hindcast over the North Atlantic are considered: *Hs*, significant wave height; T_P, peak wave period; Hs_{90}, ninetieth percentile significant wave height; Tp_{90}, ninetieth percentile of peak wave period; P_W, wave power per unit of wave crest, determined as $P_W = a\ Hs^2\ T_P$ where a is a constant [*Kinsman*, 1965; *Bromirski et al*., 2013, equation (1)]; Pw_{50}, fiftieth percentile wave power; Pw_{90}, ninetieth percentile wave power; Hs_{90T}, number of *Hs* occurrences above the ninetieth percentile level during a given season; Pw_{90T}, number of *Pw* occurrences above the ninetieth percentile level during a given season; P_E, wave power for wave events that exceed a prescribed *Hs* threshold; and P_{Emax}, maximum wave power event.

We follow the methodology presented in *Bromirski et al*. [2013], with empirical orthogonal function (EOF) analyses employed to identify the regions in the North Atlantic where *Hs* and P_W exhibit the greatest variance, and to investigate regional and basin-wide variability from the EOF patterns and their principal component (PC) time series of anomalous P_W activity. *Tp* is determined from the peak of the wave spectrum, which generally has a dominant influence on P_W. *Tp* is usually significantly higher than the mean wave period (supporting information Table V2). As describing variability of strong wave activity was one of the objectives, *Tp* was thus chosen as the wave period estimate used to compute P_w.

Linear trends in several of the identified measures were calculated over the six-decade hindcast. These trends were designated to be significantly different from zero if they met or exceeded the 95% significance level of a two-sided Student's *t* test linear regression null-hypothesis test [*Hines and Montgomery*, 1980].

3. Wave Model *Hs* Validation

The performance of the WW3 model *Hs* hindcast has been described for the North Pacific in *Bromirski et al*. [2013]. Here the performance of the WW3 model outputs is evaluated by comparison with buoy measurements in the North Atlantic. These comparisons serve as validation that model outputs are representative of wave activity, although both model outputs forced by reanalysis winds and buoy measurements include instrumental error. Detailed comparison of WW3 and National Oceanographic Atmospheric Administration (NOAA) National Oceanographic Data Center (NODC) buoy *Hs* time series over the western boundary of the North Atlantic for all available buoy data at selected locations along the U.S. East Coast spanning 1981–2008 (supporting information validation Figures V2a and V2c) and during 1998 and 2008 (V3a, V3c, V4a, and V4c) demonstrate the consistency of WW3/buoy relationships along the western North Atlantic boundary. Consistency of WW3 model *Hs* with observations in the northeast Atlantic is demonstrated with buoy data from the UK Met Office spanning 1998–2008 (Figure V7). Buoy data were used in unaltered form, as they were received from NODC and the UK Met Office. These time series plots exhibit strong agreement between *Hs* peaks in WW3 wave model and those from NOAA and UK Met buoy records, indicating that the NRA-1 model wind fields and the associated atmospheric circulation patterns are generally well determined. However, similar to the North Pacific [*Bromirski et al*., 2013], in the western North Atlantic the WW3 model *Hs* generally tend to underestimate buoy *Hs*, particularly at near-coastal locations. This is likely affected by local bathymetry and coastline configuration, the general NRA-1 underestimation of high wind events [*Swail and Cox*, 2000], and/or being at the western boundary of the model domain where winds generated by storm systems near the eastern continental margin may not be well represented. In contrast, along the eastern boundary, WW3 *Hs* is generally in good agreement with *Hs* measured by UK Met buoys both in winter and summer (Figure V7), previously observed for other wave models [*Bidlot et al*., 2002].

Scatter plots comparing WW3 and western boundary buoy *Hs* (supporting information Figures V2b, V2d, V3b, V3d, V4b, and V4d) are reasonably tight, with high squared correlation coefficients (r^2), typically >0.7, indicating that *Hs* variability is well represented by WW3 model data, with observed relationships consistent during 1998 and 2008. Scatterplot least squares slopes are less than 1, indicating that WW3 model *Hs* tend to be less than buoy *Hs* estimates, similar to model performance comparisons for the eastern North Pacific in *Bromirski et al*. [2013]. The somewhat higher r^2 values obtained in Bromirski et al. suggests that the WW3

hindcast does not model the wave climate intensity along the western boundaries as well as along the eastern boundaries, possibly because storms along and adjacent to the North American continent tend to have more limited fetch and perhaps have more erratic development than those along eastern boundaries. The strong correspondence of model-simulated waves in the western North Atlantic is confirmed by $r^2 \sim 1$ for correlations between WW3 and UK Met *Hs* (Figures V8 and V9). And as the *Hs* comparisons show, WW3 underestimates the western boundary wave climate, which is reflected in both lower wave heights and lower *Tp* (Table V1) than buoy observations.

Comparisons of WW3 and western boundary buoy Hs at both nearshore and offshore NOAA buoy locations (Figure V1) during winter (November–March, Figures V5a and V5b) and summer (May–September, Figures V5c and V5d) seasons over the 1981–2008 epoch, and at UK Met locations (Figure V6) during winter and summer (Figure V10) over each year during the 1998–2008 epoch have similar relationships to those obtained by *Bromirski et al*. [2013] for the eastern North Pacific. Climatological *Hs*, obtained for all available data at UKMet Office Northeast Atlantic buoy 62108 and at NOAA buoy 44011 in the western North Atlantic (supporting information Figure V12), indicate that the monthly mean *Hs* during November is higher than during March at 62108, while the opposite is the case at 44011. Thus, in order to ensure that most strong *Hs* events were included in our analyses, November–March were chosen as the winter season. May–September were chosen as a corresponding 5 month summer period that includes months with generally the lowest wave activity. Additionally, the choice of winter months corresponds to the North Pacific index [*Trenberth and Hurrell*, 1994] and follows *Bromirski et al*. [2013] for ease of comparison between the North Atlantic and North Pacific basins.

Although the year-by-year slope of the regressions between model and buoy *Hs* show substantial interannual variability, the lack of statistically significant trends in the regression coefficients suggests that the WW3 model *Hs* are self-consistent. Given that the regression fit does not change consistently over the buoy record period, additional satellite data available in the later part of the NRA reanalysis does not seem to create a spurious trend in the waves. The generally high correlations between WW3 and buoy observations reflect the strong association of heightened wave activity that are associated with broad-scale atmospheric circulation patterns that influence storminess along the U.S. East Coast [*Hirsch et al*., 2001] and along the coasts of Scotland and Ireland [*Woolf et al*., 2002].

Because *Tp* is determined from the peak of the wave spectrum, i.e., the frequency band that provides the largest contribution to *Hs*, comparisons of model and buoy *Hs* are directly linked with *Tp*. *Hs* comparisons show a consistently large *Hs* underestimation along the western boundary. Consequently, it would be expected that *Tp* and P_w are also underestimated there. This was investigated for strong wave events along the western boundary (supporting information Figure V11). There is considerable scatter in mean *Tp* for strong wave events, with buoy *Tp* typically about 30% larger than model *Tp* (Figure V11a). The combination of *Tp* and *Hs* model estimates yields model P_w estimates that are on average 50% less than the buoy observations (Figure V11b). Unfortunately, *Tp* was not available from the UK Met Office, so east-west model *Tp* and P_w performance comparisons are not possible. However, given the much better correlation between model and buoy *Hs* in the northeast Atlantic, the respective differences between model and buoy *Tp* and P_w are presumably substantially less there.

4. Wave Power Spatial and Temporal Patterns and Climate Associations

4.1. Spatial Distribution

The seasonal patterns of *Hs*, *Tp*, and P_W, having daily levels at or exceeding the ninetieth percentile level, aggregated over the period of record, are useful to gage and interpret variations and trends of the higher extremes of these measures (Figure 1, ninetieth percentile; Hs_{90}, Tp_{90}, and Pw_{90}, respectively). It should be noted that mean P_w obtained with *Tp* is larger than the mean wave power that would be obtained using mean wave period. The Hs_{90} pattern is similar to that determined by *Wang and Swail* [2001] over the 1958–1997 epoch. The maxima of both Hs_{90} and Pw_{90} in winter and summer are centered near 57°N, 342°E, located in the northeast Atlantic south of Iceland. The peak in Pw_{90} is somewhat to the east, in part from progressively higher *Tp* eastward (Figure 1c) within the presumably dominant wave generation region in the higher latitudes (about 45°N–62.5°N) across the North Atlantic. The wave period associated with strong wave energy, represented by Tp_{90}, increases eastward and southward, away from the dominant generation

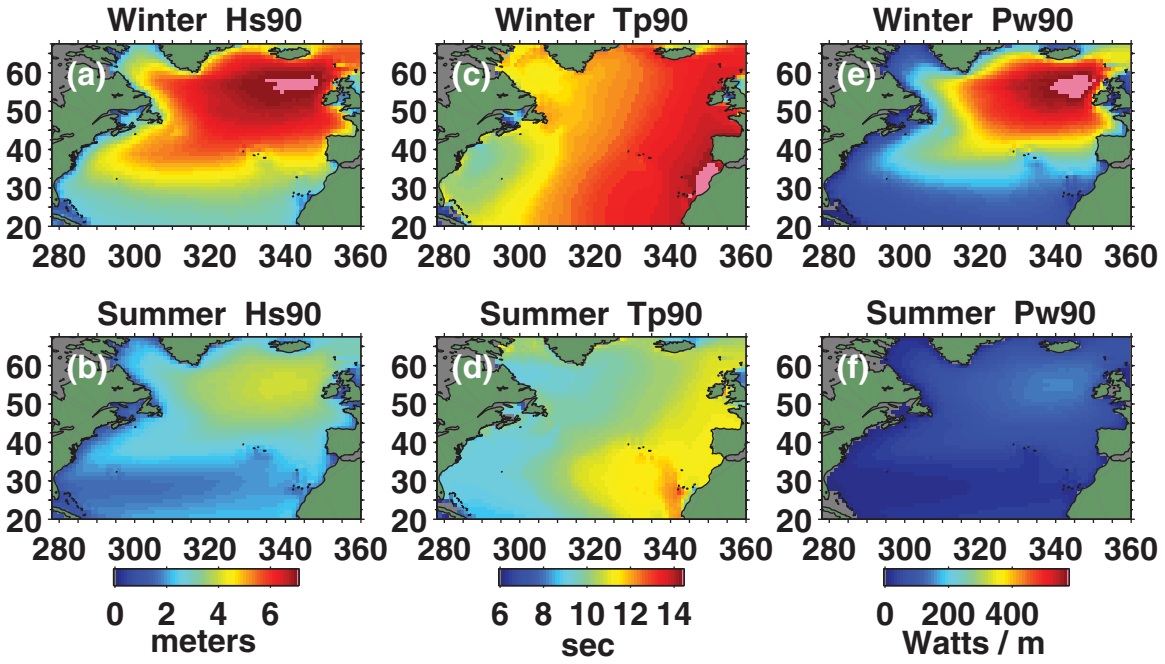

Figure 1. Distribution of ninetieth percentile *Hs*, *Tp*, and P_W during winter (top row, November–March) and summer (bottom row, May–September) seasons.

region. The shadowing effect of the Azores Islands for waves propagating from the north is evident in Figure 1.

In winter and summer, the spatial distributions of more extreme wave heights and wave power, characterized by the 98th percentile level (spatial variability in supporting information Figure S1), are similar to their ninetieth percentile patterns in Figure 1, however with maxima in Hs_{98} and Pw_{98} (Figures S1c and S1k) located somewhat eastward of Hs_{90} and Pw_{90}, closer to the coasts of Ireland and Scotland.

In summer, less intense and less spatially extensive storms produce lower *Hs* and reduced long-period wave energy. Peaks in summer Hs_{90} and Pw_{90} (Figures 1b and 1f) are approximately colocated, somewhat south and west of their winter locations (Figures 1b and 1f). The summer Hs_{90} peak is only a little more than half that during winter, consistent with the fact that summer Pw_{90} is less than a third of winter levels, similar to that observed for the North Pacific [*Bromirski et al.*, 2013]. The summer Tp_{90} pattern is influenced by both extratropical and tropical storm (hurricane) activity. However, the 1.0° × 1.0° latitude and longitude resolution of this hindcast is insufficient to resolve waves from relatively fast-moving small-area hurricanes and storms [*Tolman*, 2006]. In addition, *Swail and Cox* [2000] showed that tropical storms are poorly resolved in the NRA wind fields, resulting in substantial underestimation of tropical storm-generated waves.

4.2. Spatial Patterns of Anomalous P_W: Proximity to Coasts

Wave power, P_W, depends strongly on the square of wave height, so P_W EOF spatial patterns are expected to be similar to *Hs* EOF patterns [*Bromirski et al.*, 2013]. However, P_W also depends on peak wave period, T_P, which depends on storm size and associated longer fetch dimension, intensity, and duration. Consequently, P_W more fully describes storm and wave energy variations, and changes, and better characterizes storm wave activity across the North Atlantic. P_W is particularly relevant to wave impacts along coasts, especially because wave runup, the vertical height above a still-water reference level reached by incident waves at the shore, increases with higher *Hs* and longer *Tp* [*Stockdon et al.*, 2006]. Anomalous monthly P_W, determined from the difference between the P_W monthly mean and climatological mean at each grid point, is used to characterize P_W spatial variability.

The dominant pattern of P_W variability across the North Atlantic over the entire WW3 record (1948–2008), represented by EOF 1, is characterized by a dipole pattern (Figure 2a), with the dominant pole focused about 5° west of Ireland extending westward to the mid-northeast Atlantic accompanied by a weaker pole

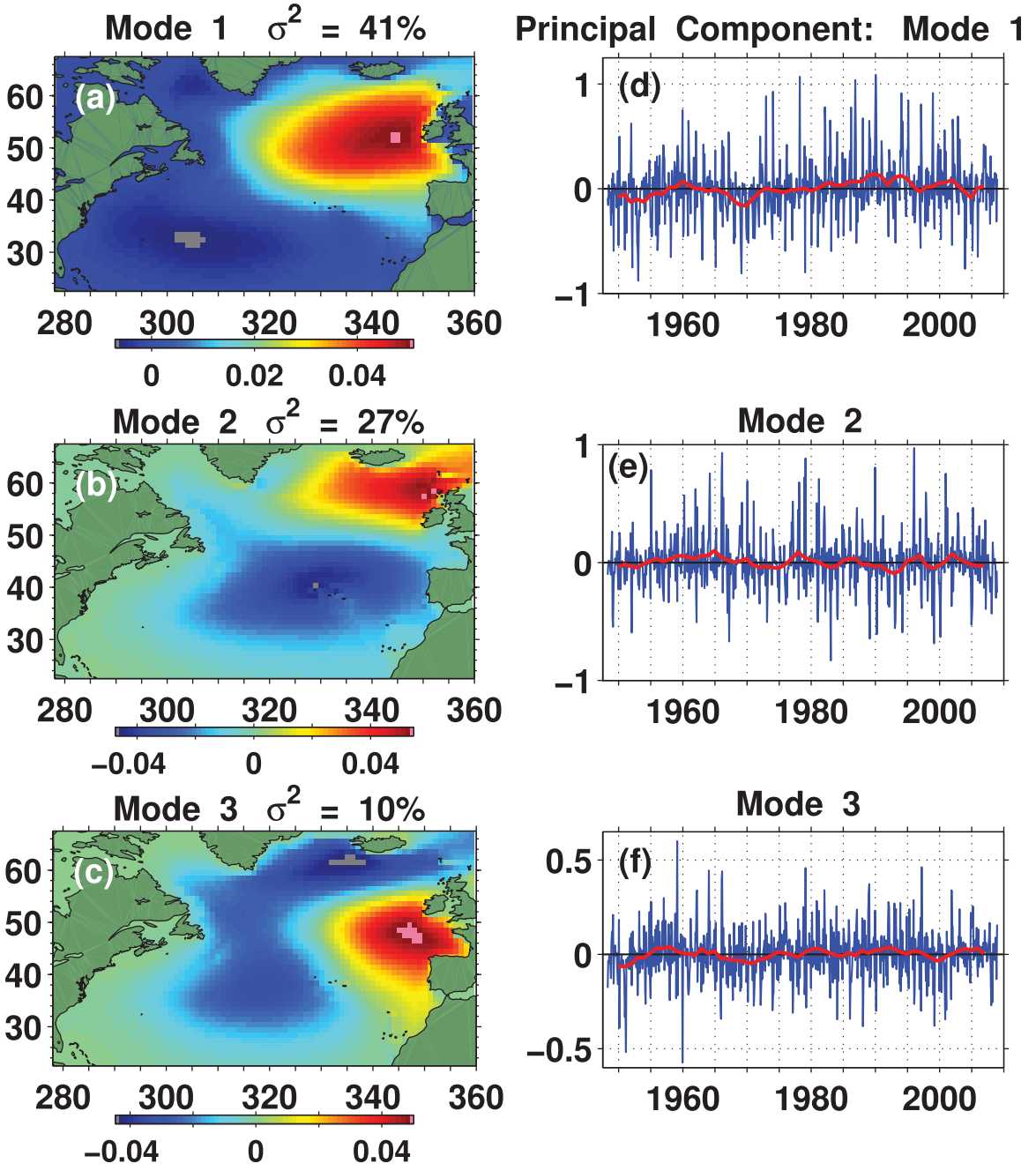

Figure 2. Spatial and temporal wave power, *Pw*, variability over the entire 1948–2008 time period described by (a–c) empirical orthogonal function (EOF) patterns and (d–f) associated principal components (PCs, with 3 year running means (red lines)) for the first three modes. These were determined from monthly *Pw* anomalies (formed from the difference between the monthly mean and the climatological mean at each grid point) normalized to unit variance. Positive PC excursions are associated with the red spatial patterns. The variance, σ^2, accounted for by each mode is given in Figures 2a–2c.

centered to the southwest near 33°N, 305°E. This dipole pattern is similar to that observed in the NAO, the leading anomalous atmospheric pressure mode in the North Atlantic region [*Barnston and Livezey*, 1987]. The first three P_W modes (Figures 2a–2c) account for 78% of the variance, as opposed to about 65% accounted for by the first three *Hs* modes (supporting information Figure S2). P_W mode 1 has a spatial pattern that resembles *Hs* mode 1, but the dominant P_W pole is shifted about 5° closer to the Ireland west coast and accounts for substantially more of the variance than *Hs* mode 1 (41 versus 31%, respectively). The P_W mode 2 (Figure 2b) also exhibits a dipole-pattern, but shifted to the north and east of mode 1. The strong dipole patterns for EOF modes 1 and 2 are similar to those for seasonal trend patterns (Figures 3 and 4),

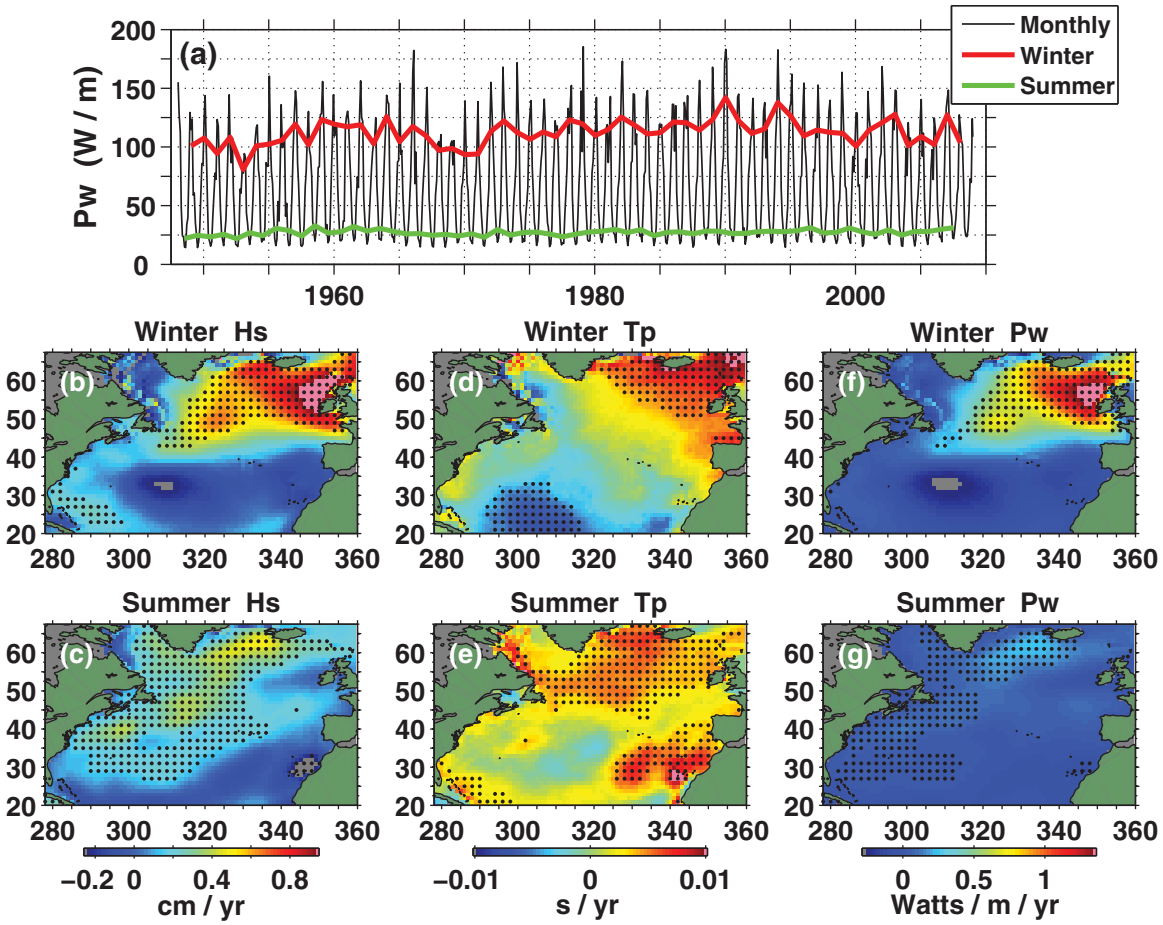

Figure 3. (a) Basin-wide mean P_W averaged on monthly and seasonal time scales. (b–g) Seasonal trends in *mean Hs*, *Tp*, and P_W during (middle) winter (November–March) and (bottom) summer (May–September) seasons over the 1948–2008 epoch. Some regions gray (pink) either lack data or had trends less (greater) than the minimum (maximum) range indicated. Trends significantly different from zero at the 95% level at a minimum of 3 of 4 grid nodes in 2° × 2° (lat, long) regions are indicated by black dots centered within respective regions. The regional trend significance identification methodology applies to all subsequent similar figures.

although the strong dipole is not reflected in the percentile distributions (Figure 1 and supporting information Figure S1).

In contrast to modes 1 and 2, the P_W mode 3 dipole has its dominant pole centered south of Ireland, with an out-of-phase, horseshoe-shaped anomaly to the north, west and south from Iceland to the central North Atlantic. Mode 3 may be associated with more southerly North Atlantic storm tracks during the negative phase of the NAO (to be discussed below). The P_W mode 3 eastern pole would tend to have its strongest influence associated with wave activity along the coasts of France, Spain, and Portugal. The three P_W modes shown in Figure 2 are all associated with anomalous wave energy along the Atlantic coast of Europe, but the wave activity represented by each is oriented along a different latitude zone.

4.3. Principal Components

The monthly to multidecadal variability of wave power EOF modes is given by the principal components (PCs) associated with P_W EOF modes (Figures 2d–2f). P_W PC1 shows a significant increase in the occurrence of high amplitude positive values after the early 1970s, consistent with enhancement during the positive phase of the NAO, discussed below. Additionally, as indicated by the 3 year running means, P_W PC1 roughly conforms to the NAO state, e.g. 1965–1970 (negative) and 1990–1995 (positive). Note the generally diminishing variance and amplitude of PC mode 1 levels (characterized by the 3 year running means) after the mid-1990s when the NAO is generally decreasing, and correspondingly generally negative PC1 prior to 1970 when the NAO is negative. These relationships are further emphasized by winter PC1 (supporting information Figure S3d). PC2 represents a subtle shift in wave power closer to the eastern boundary. The

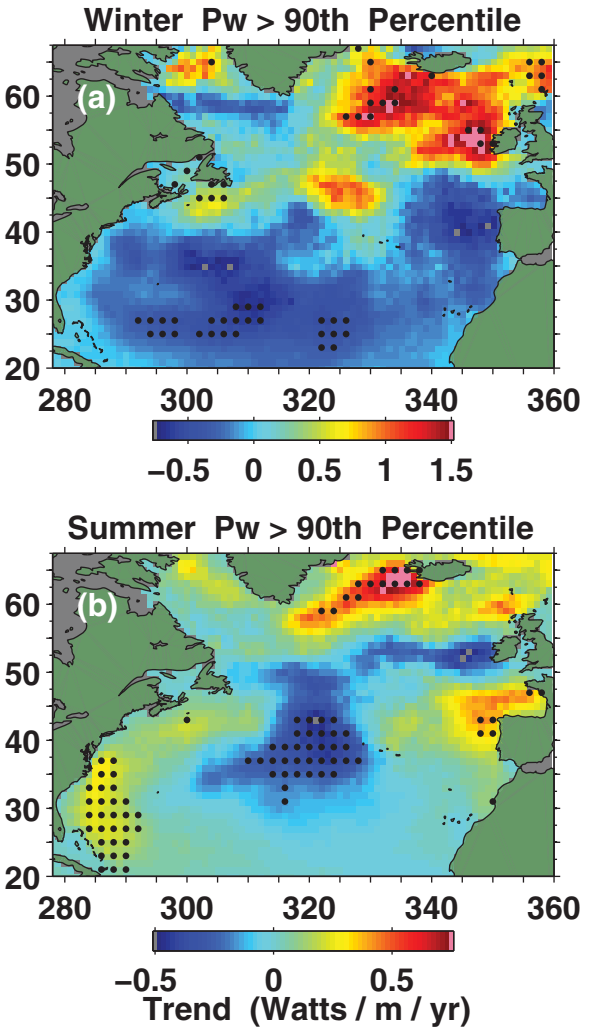

Figure 4. Trends in Pw_{90T}, the mean *Pw* exceeding the ninetieth percentile level during (a) winter (November–March) and (b) summer (May–September) seasons. Trends that pass the 95% significance test at 2° × 2° (lat, long) regions are indicated by dots. Note that the range in Figure 4a is about twice that in Figure 4b.

relatively subtle differences between the first three modes reflect a transition toward heightened wave activity across the northeast Atlantic during the positive phase of the NAO, as will be described in subsequent sections.

4.4. Basin-Scale P_W Climate Associations

Modes of climate variability that have been demonstrated to influence North Atlantic storm activity include the North Atlantic Oscillation (NAO) [*Hurrell*, 1995] and the Arctic oscillation (AO) [*Thompson and Wallace*, 1998; *Deser*, 2000], with the NAO considered to be the North Atlantic regional expression of the northern annular mode AO. In addition, studies [e.g., *Wallace and Gutzler*, 1981; *Honda and Nakamura*, 2001; *Franzke et al*., 2004; *Wettstein and Wallace*, 2010] indicate there is an association of North Atlantic winter storm and wave activity with North Pacific climate variability, characterized by the Pacific North America pattern (PNA) [*Wallace and Gutzler*, 1981] and the North Pacific pressure pattern (NP) [*Trenberth and Hurrell*, 1994], and SST-derived indices NINO3.4 [*Kumar and Hoerling*, 2003] and the Pacific Decadal Oscillation (PDO) [*Mantua et al*., 1997].

Climate associations with basin-wide North Atlantic P_W were determined by correlating P_W PCs with the NAO, AO, PDO, PNA, and NINO3.4 climate indices (Table 1). As might be expected, the highest correlations of winter P_W PCs are with atmospheric circulation indices NAO and AO. In fact PC1–3 are all positively and significantly correlated with NAO and AO during winter. The similarity of NAO and AO correlations during winter is consistent with their close association [*Thompson and Wallace*, 1998; *Deser*, 2000; *Thompson and Wallace*, 2000]. The somewhat better correlation of PC1 with NAO compared with AO likely results from the inclusion of remote

Table 1. Correlation of Basin-Wide PCs of Mean Seasonal *Pw* With Climate Indices[a]

	NAO			AO			PDO		PNA		NINO3.4	
Mode	1	2	3	1	2	3	1	2	1	2	1	2
Winter (Nov–Mar): % variance$_{1,2,3}$ = 42, 28, 9												
	0.64	**0.71**	**0.28**	**0.59**	**0.67**	**0.44**	0.20	−0.15	0.01	−0.14	0.10	−0.14
Summer (May–Sep): % variance$_{1,2,3}$ = 39, 21, 11												
	0.17	**0.55**	**0.28**	0.21	**0.34**	0.14	0.01	−0.19	−0.02	−0.22	0.02	−0.13
Full year (all data): % variance$_{1,2,3}$ = 41, 27, 10												
	0.37	**0.50**	−0.02	**0.47**	**0.51**	0.07	0.04	**−0.07**	**−0.10**	0.00	0.06	−0.06

[a]Correlation coefficients, *r*, for the mean seasonal monthly anomaly P_W principal components of modes 1, 2, and 3 (% variance given in subheadings) of *Pw* anomalies over the North Atlantic from 20°N to 70°N versus average winter and summer NAO, AO, PDO, PNA, and NINO3.4 indices, 1948–2008. Also included are correlations form using monthly anomalies over all months of the year, 1948–2008 (see Figure 5). Correlations with *p* values ≤0.05 are bold.

atmospheric variability not directly affecting the North Atlantic in determining the AO. The closer association of P_W with NAO is a consequence of its determination from the sea level pressure difference between the Icelandic low and the Azores high, which preferentially focuses on northeastern Atlantic variability. None of the three P_W PC's is correlated with any Pacific climate modes because the North Atlantic P_W modes are not strongly weighted in the western North Atlantic.

During summer, P_W PC correlations (Table 1) indicate that summer P_W variability, like that in winter, is most closely correlated with the NAO, although at somewhat lower levels than in winter. Of particular interest is that in summer NAO and AO are correlated significantly with P_W mode 2, but not with mode 1, evidently reflecting a shift in the storm track in summer that relates to NAO. The diminished correlations in summer are consistent with the lack of similarity of PC1 variability to the NAO during summer compared with winter PC1 (compare supporting information Figures S3d and S4d). Other factors are also likely involved, i.e., a stronger influence of climate patterns other than NAO and AO, such as tropical cyclone activity and smaller scale weather and climate influences, are affecting P_W variability during summer. Weak or negligible correlation with North Pacific based climate indices PNA (and NP, not included), PDO, and NINO3.4 during summer suggests that these modes of North Pacific climate variability have minimal influence on storm activity over the North Atlantic.

5. H_S, T_P, and P_W Trends Across the North Atlantic

Wave activity in North Atlantic varies considerably from month-to-month and year-to-year, as represented by the time series of average wave power aggregated over the entire North Atlantic north of 15°N (Figure 3a). On a monthly average basis during the winter period the basin-wide aggregated wave power fluctuates by a factor of 10 or more with highest values being 3σ above the mean, while from year-to-year winter P_W can be 75% greater than the winter mean. Also, there is a trend toward higher winter wave power, by about 12% from the late 1940s to the late 2000s. Mean winter NAO exhibits peaks that are generally associated with elevated winter P_W, with differences likely resulting from wave activity in the western and southern part of the basin where the NAO has minimal influence. Summer mean P_W is significantly lower than winter by factors of from 4 to 7, and exhibits much less interannual variability. The following are results from a further investigation of P_W trends.

5.1. Winter and Summer Trends

Long-term changes in winter and summer wave activity were explored by computing trends in seasonal mean *Hs*, *Tp*, and P_W over 1948–2008. During winter, statistically significant upward trends in mean *Hs* and mean P_W (Figures 3b and 3f) are observed at most locations north of 45°N, dominated by increasing wave activity in the northeast Atlantic [e.g., *Wang and Swail*, 2001]. This broad scale increase in P_W reflects an increase in the NRA-1 westerly winds poleward of about 40°N, suggesting that over the 1948–2008 time span there was an intensification of winter storm activity over the eastern North Atlantic. This intensification is described later in regards to NAO changes.

Significant trends in mean P_W at many locations north of 45°N in Figure 3f amount to P_W increases of more than 25% during winter over the entire 60 year record compared with mean PW_{50} levels in this region (shown in supporting information Figure S1i), further described in a regional analysis below. The locations of strongest upward trends in winter *Hs* and winter P_W (Figures 3b and 3f) are both east of the peaks in their climatological mean ninetieth percentile patterns (Figures 1a and 1e), nearer the western coasts of Ireland and Scotland. Although not significant, there are decreasing trends in winter *Hs* and winter P_W south of about 40°N. The dipole patterns of trends in winter *Hs* and P_W, particularly the increasing trends north of 45°N, are reflective of the shift in winds over the North Atlantic associated with change toward a stronger NAO circulation [*Barnston and Livezey*, 1987]. Upward trends in the winter mean of peak wave period, *Tp*, occur over the northeast Atlantic (Figure 3d), indicating increasing mean winter storm intensity in this region during later epochs. The general pattern of trends in winter P_W, *Tp*, and *Hs* is consistent with that shown previously *Wang et al*. [2009] indicating increasing *Hs* at higher latitudes and decreasing *Hs* at more southerly latitudes. Particularly important from a societal perspective are upward trends along the Atlantic coast of Europe.

During summer months, in contrast to winter patterns, significant although generally weak upward trends in both mean *Hs* and P_W are found in some regions of the western North Atlantic (Figures 3c and 3g), with upward trends in *Tp* over most of the North Atlantic north of 45°N. The patterns of significant upward

trends are quite broad presumably reflecting regional increases in summer storm intensity. Although relatively small, the upward trends are generally positive along the U.S. Atlantic coast, indicating that even during summer months North Atlantic storm activity has undergone regional increases. Tropical cyclone activity likely influences the upward summer trends observed south of 45°N, particularly for *Tp* west of Africa and Portugal.

5.2. Hs_{90} Exceedance Patterns

Variations and long-term increases in mean wave activity are an important indicator of a fluctuating wave climate, but changes in the occurrence of the higher amplitude portion of the *Pw* distribution are especially significant from a coastal impacts perspective. From a tally of all *Pw* occurrences above the ninetieth percentile level, Pw_{90T}, at each grid node during winter and summer, the seasonal trends were determined. Trends in Pw_{90T} during winter months (November–March, Figure 4a) exhibit a pattern similar to mean *Pw* seasonal trends (Figure 3f). Notable features in Figure 4a are (1) strong increases in winter Pw_{90T} along the west coast of Ireland, (2) moderate increases south of Nova Scotia, and (3) significant downward trends across much of the North Atlantic south of 30°N, consistent with trends in winter *Hs* and P_W in Figure 3 and with results shown by *Wang et al*. [2009] and *Wang and Swail* [2001].

Summer Pw_{90T} trends (Figure 4b) show significant increases in a swath to the southwest of Iceland, and decreases in the central North Atlantic. However, summer mean *Hs* (Figure 3c) has significant, although weak, upward trends in the central North Atlantic, indicating that although the summer mean *Hs* is increasing, the highest wave activity, characterized by Pw_{90T}, is not. In contrast, the southwestern North Atlantic and along the west coast of Portugal shows significant upward Pw_{90T} trends (Figure 4b), which may a recent surge in hurricane activity [*Bromirski and Kossin*, 2008].

6. Strong Wave Power Events (P_E)

6.1. Event Wave Power

Clearly the seasonally aggregated wave effects are orchestrated by large-scale atmospheric circulation patterns, but strongest wave impacts along coasts are dictated by cyclone tracks and associated high winds during individual storm events. Both T_P and wave event duration are important factors in estimating the potential for coastal impacts. Following *Bromirski et al*. [2013], the wave power integrated over a storm event, P_E, at each grid node is determined from

$$P_E = \int_0^\tau P_W dt, \tag{1}$$

i.e., the integral of P_W over the wave event duration, τ. Because P_E results from both H_S and T_P wave parameters, P_E provides a more complete measure than H_S alone of the potential for storm waves that can cause the greatest coastal impacts.

Here as in *Bromirski et al*. [2013], wave events are defined as H_S being continuously above a prescribed threshold for at least 12 h. Since the most extensive damage to coastal infrastructure occurs when high waves occur near high tide, the 12 h event criterion ensures that waves at some time during a given events will coincide with a high tide, although potentially not during the highest diurnal level. These event identification criteria allow us to characterize changes in the incidence and spatial variability of strong storm-wave events. Since the WW3 model's time resolution is 6 h, three consecutive H_S estimates above threshold thus give an effective τ for extreme events of at least 12 h. The ninetieth percentile threshold at each grid node was employed as in *Bromirski et al*. [2013], which effectively includes all high-energy events.

Trends in storm event wave power, P_E, were determined from the time series formed from each year's seasonal mean of all P_E events at each grid point. Each event is defined at each grid point by *Hs* exceeding the seasonal (winter or summer) spatially variable Hs_{90} level for at least three consecutive realizations (12 h). The number of events and the duration of each event were also considered. Examination of trends in the largest event in each season is also presented.

6.2. Trends in P_E

Changing climate patterns affect atmospheric circulation and associated wind patterns that generate ocean waves. Trends in wave amplitudes over the North Atlantic reflect changes in cyclone frequency and

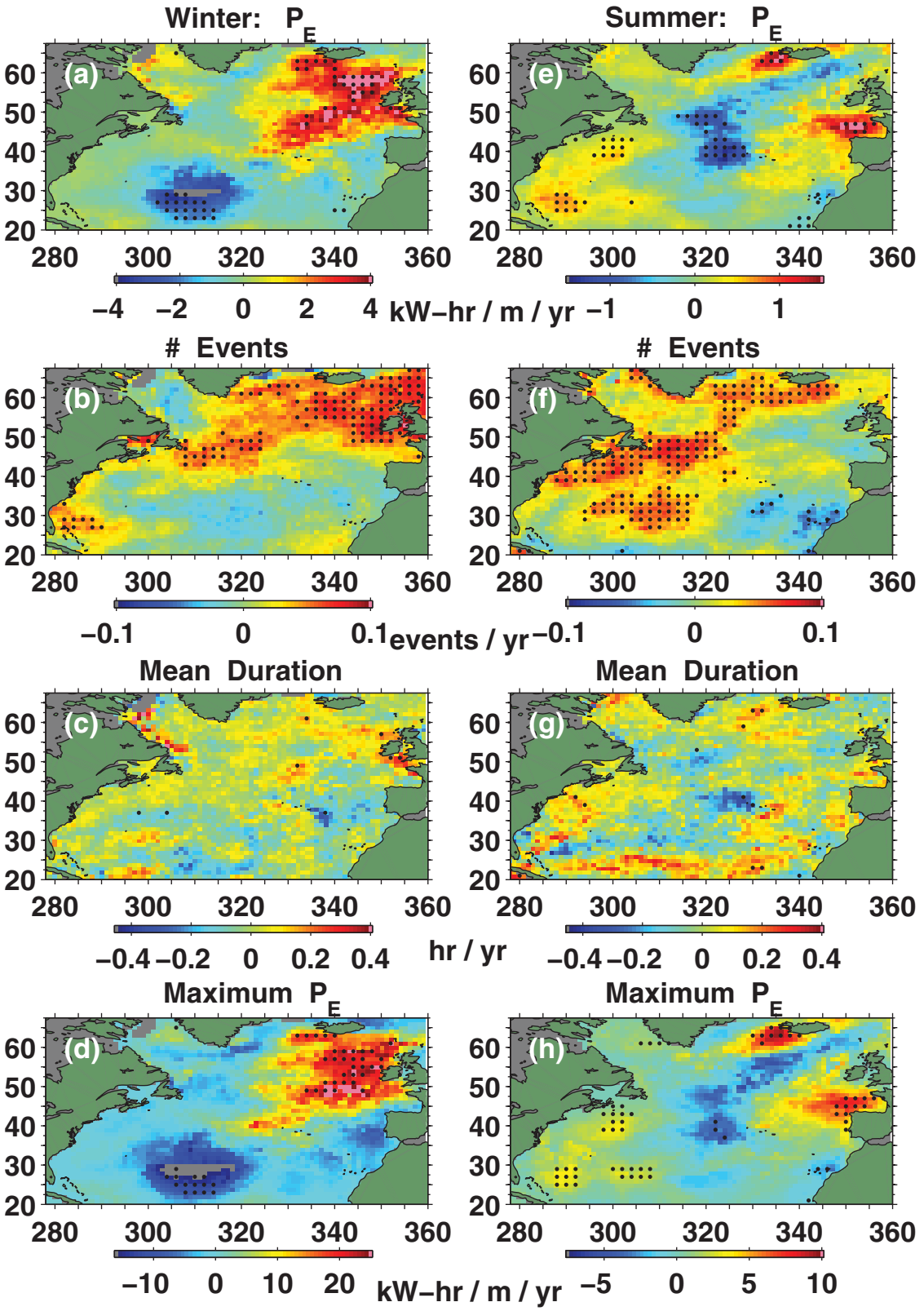

Figure 5. Trends in characteristics of mean event wave power, P_E, during (a–d) winter and (e–h) summer seasons over the model record (1948–2008) determined for all events during respective seasons. (bottom) Trend in the maximum P_E event amplitude during the two seasons. Events were defined at each grid node by *Hs* continuously exceeding the ninetieth percentile threshold at least three consecutive realizations (12 h duration). Some regions in gray either lack data or had trends less than in gray (greater than; pink) the minimum (maximum) range indicated. Trends that pass 95% significance test over 2° × 2° (lat, long) regions are indicated by dots, as in Figure 3.

intensity [*McCabe et al*., 2001; *Geng and Sugi*, 2001; *Hoskins and Hodges*, 2002; *Wang et al*., 2006]. Realizing that trend estimates determined here are derived from model estimates that have inherent uncertainties, identification of the regions with significant trends over 1948–2008 are perhaps more meaningful than the magnitude of associated trends, which if steep are unlikely to be sustained over an extended time period.

6.2.1. Trends in Winter P_E

The pattern of significant trends in winter P_E (Figure 5a) is similar to that of winter Hs_{90T} trends (Figure 4a), as expected, since changes in the highest waves are driven by the largest individual events. The strongest significant upward trends in winter P_E occur in the region of strongest PW_{90} trends in the western North Atlantic (Figure 3b), with an elongated region extending southwest of Ireland that is likely associated with prevailing storm track [*Hoskins and Hodges*, 2002]. These strong P_E trends are approximately colocated with the northeastern dominant poles of the P_W mode structure (Figure 2), which have a strong connection to NAO and AO (Table 1), particularly during winter. A combination of factors (number and duration of events) underlies the strength of trends in these regions. Storms and wave energy in mid and higher latitudes generally propagate eastward, resulting in the upward trends in P_E observed along the Atlantic coasts of Iceland and the British Isles, along with much of the European Atlantic coast. The negative part of the trend dipole is a patch of diminished winter P_E in lower latitudes of the central North Atlantic between 25°N and 35°N, centered near the southern secondary pole of the North Atlantic P_W EOF dipole structure (Figure 2a).

6.2.2. Trends in Summer P_E

The pattern of summer (May–September) P_E trends (Figure 5e) is closely aligned with summer Hs_{90T} (Figure 4b). During summer, upward trends are not statistically significant over much of the North Atlantic. However, upward trends do occur in isolated regions in the western North Atlantic, near Iceland, and near the Bay of Biscay, consistent with *Charles et al*. [2012]. The upward trends observed are generally less than half the magnitude of those during winter, an indication of the generally weaker variability that occurs in summer.

6.2.3. Trends in the Number of Winter P_E Events

In contrast to the changes in the overall *magnitude* of winter P_E events, which were concentrated in the eastern North Atlantic, the *number* of winter P_E events exhibits a somewhat broader pattern of increase over 1948–2008 (Figure 5b). In addition to the northeast Atlantic, the increases are found across regions of the western North Atlantic off the coasts of Florida and the Carolinas and east of Nova Scotia. The magnitude of the upward trends in these regions is approximately equivalent to one additional strong wave event each winter for each decade of the record, similar to that observed for the North Pacific [*Bromirski et al*., 2013].

6.2.4. Trends in the Number of Summer P_E Events

Increases in the number of summer P_E events are concentrated in the central and western regions of the basin (Figure 5f). Significant upward trends in the number of summer P_E events occur along the U.S. New England coast. Increasing numbers of summer P_E events in this coastal region and in the south-central portion of the basin, about one additional strong event each summer per decade as during winter, are likely partly the result of increasing tropical cyclone-generated wave activity [*Bromirski and Kossin*, 2008].

6.2.5. Trends in Mean Duration of P_E Events

Besides changes in intensity and frequency, another characteristic of interest is changes in duration of P_E events, which were determined from the mean of all events for each year during each season. Except at isolated locations, winter mean P_E duration has not increased over most of the North Atlantic basin (Figure 5c), and most increases failed to qualify as statistically significant. Although significant upward trends in winter mean P_E duration occurred over isolated locations near the British Isles (Figure 5c), the lack of spatial consistency and the potential strong influence of anomalous events during individual winters raises the possibility that may be artifacts of the processing methodology or spurious wind field estimates [*Chang*, 2007; *Sterl*, 2004].

6.2.6. Trends in Yearly Maximum P_E Winter Season

Increases in extratropical cyclone (ETC) intensity and associated extreme wave heights over the period from about 1958 to 2000 have been identified across the North Atlantic [*Wang and Swail*, 2001; *Wang et al*., 2006, 2008], with greatest increases concentrated in the mid-to-high latitudes. Probably, the increasing trends in ETC intensity are linked to increases in mean and number of P_E events described above. Additionally, ETC

intensity increases should result in increasing magnitude of extreme P_E events, which is tested by mapping trends in each year's winter maximum wave power event, P_{Emax}, at each grid node.

As would be expected, regions having strongest upward trends in winter P_{Emax} (Figure 5d) are colocated with the regions with the largest mean winter P_E increase (compare Figure 5d with Figure 5a). Significant upward trends in P_{Emax} over the eastern mid-latitudes between 45°N and 65°N occur in conjunction with significant increases in the occurrence of strong events in this region (Figure 5b). Most notable from a coastal impacts perspective are the significant upward trends in winter P_{Emax} along the western coasts of Iceland and Ireland. To the southwest, decreases in the yearly maximum winter P_{Emax} appear near 30°N, colocated with downward trends in the overall mean winter P_E.

6.2.7. Trends in Yearly Maximum P_E Summer Season

In summer, the P_{Emax} trend pattern (Figure 5h) is similar to that of summer P_E (Figure 5e), showing significant increases near the west coast of Iceland and the Bay of Biscay. Interestingly, the west coast of Iceland registers an intensified wave climate during both winter and summer.

7. Regional Variability and Associations

7.1. Regional Variability and Trends

To further describe anomalous North Atlantic wave activity, variability of P_W was investigated over a set of key regions across the basin (Figure 6a). As background, comparing the pre and post-1976 epochs, winter P_W averaged across the North Atlantic north of 15°N increased about 9%, presumably reflecting increased storm activity associated with the generally positive NAO (Table 1) after the early 1970s [*Hurrell*, 1995]. A major portion of this increase can be attributed to increases of P_W over the northeast Atlantic.

Changes in P_W are not only vital to understand the spatial and temporal makeup of wave impacts over the North Atlantic but also useful in diagnosing climate variability and possible changes in storm patterns. Monthly P_W anomalies were determined as the difference between the monthly mean and long-term climatological mean at each grid point. During winter, the strongest monthly winter P_W upward trends occur along the coasts of Ireland and Scotland (Figure 6a). During summer, of note is the comparatively steep upward trend off the western coast of Iceland (Figure 6b).

Over the entire North Atlantic, monthly basin-averaged P_W anomalies (Figure 6c) show peaks that generally correspond to P_W PC1 (Figure 2d), and reflect the general increase in P_W that occurred after the early-1970s transition to positive NAO. Increased P_W over the basin is dominated by winter wave activity, with extreme monthly basin-P_W primarily occurring during strongly positive NAO winters (Figure 6c, black curve). The influence of the NAO is evident by generally elevated winter P_W during the positive NAO (Figure 6c, red curve), e.g., during the early to mid-1990s, and of lower P_W during the negative phase, in particular during the 5 year period prior to the early 1970s transition from negative-to-positive NAO. Importantly, the tendency for lower North Atlantic wave power after the early 2000s occurs in synch with a transition toward more negative NAO (see https://climatedataguide.ucar.edu/climate-data/hurrell-north-atlantic-oscillation-nao-index-station-based).

Seven ocean regions (boxes in Figure 6a, R1–R7) were selected to investigate regional P_W variability identified in Figures 1–5 in the open ocean, and in important coastal regions. During winter, all northern Atlantic regions (R5, R6, and R7) show statistically significant upward trends (Figures 6a and 6e), reflecting increasing storm intensity that is associated with the NAO. The northernmost regions R5 and R6 have the highest mean winter P_W (Figure 6e), with magnitudes generally more than 5 times greater than those along the U.S. East Coast, although this difference may be accentuated by the greater underestimation of modeled wave activity along the western boundary (see supporting information Figure V5) compared to eastern boundaries [*Bromirski et al.*, 2013]. Substantial winter interannual variability is observed over most regions but is much less over western North Atlantic regions R1, R2, and R3 (Figures 6a and 6d), where no significant increasing trends are observed. Interestingly, a significant downward trend in anomalous P_W is observed over south-central R4, associated with the negative pole in Figure 2a and decreasing trends in P_W in Figures 3f, 5a, and 5d.

During summer, significant upward trends in anomalous P_W shift eastward (Figure 6b), with the steepest trends west of Iceland. Thus the west coast of Iceland has experienced increasing P_W virtually year round.

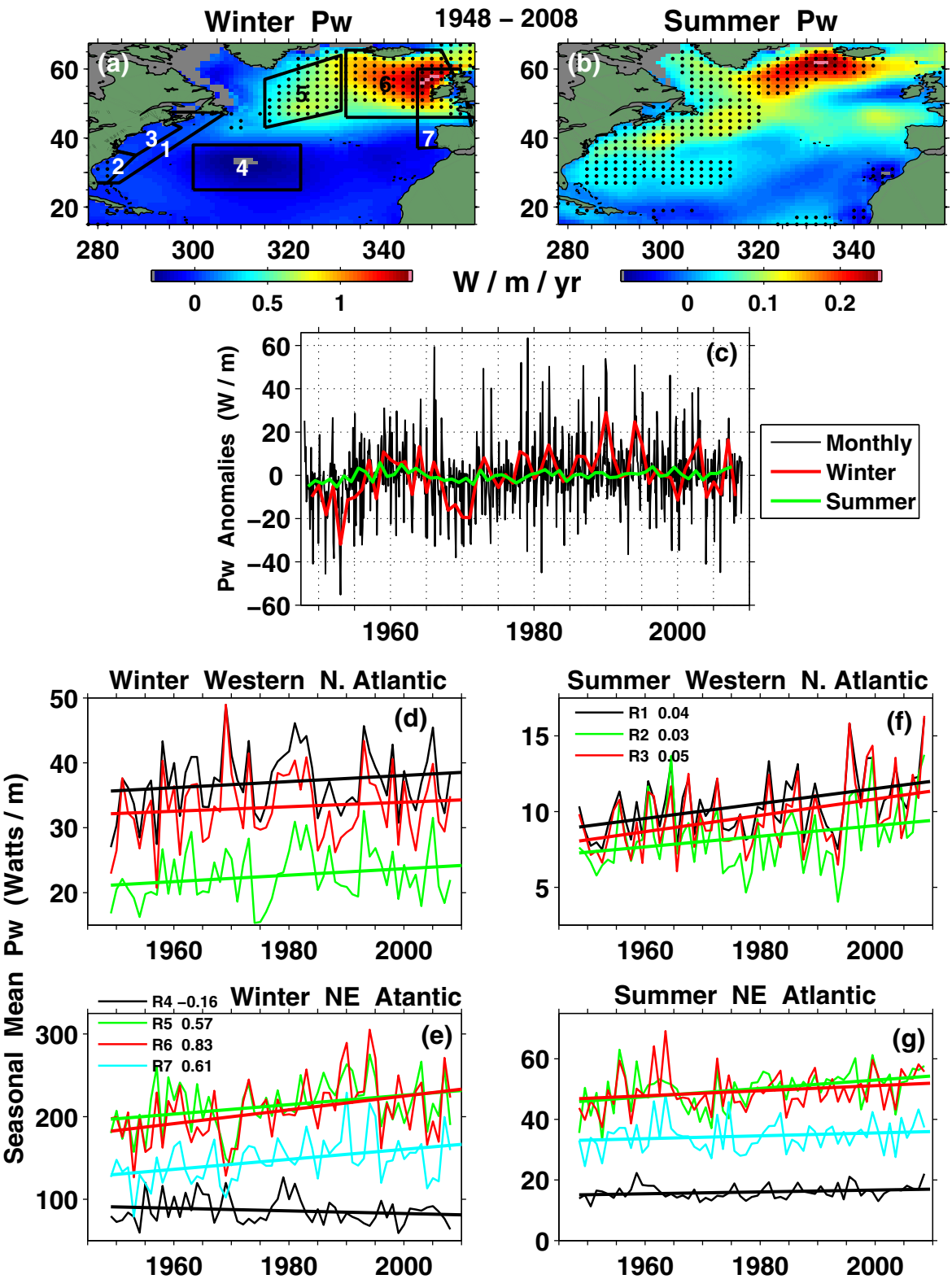

Figure 6. Variability and trends of seasonal averages in anomalous wave power across the North Atlantic 1948–2008 during (a) winter (November–March) and (b) summer (May–September) months (note different trend scales in Figures 6a and 6b, selected to enhance seasonal trends), with averages over the entire domain north of 15°N. (c) Trends over 2° × 2° boxes in Figures 6a and 6b that are significantly different from zero at the 95th level are indicated by dots, as in Figures 3 and 5. Regional (averaged over boxes delineated in Figure 6a) mean wave power during winter over (d) western North Atlantic and (e) central and northeastern Atlantic regions (see legends). (f, g) Same as Figures 6d and 6e except for summer months. R1 encompasses R2 and R3. Associated mean wave power trends (W/m/yr) are shown in Figures 6f and 6e, with trends in Figures 6d, 6f, and 6g less than 0.13 W/m/yr. Note that vertical scales differ significantly. The steepest regional trends in Figure 6e are all significant. In Figure 6f, all upward trends, although weak, are significant, while in Figure 6g, only the steepest trend over R5 (green curve, 0.13 W/m/yr) is significant. Legends in Figures 6f and 6e apply to Figures 6a and 6g, respectively.

Table 2. Correlation of Basin-Wide P_W Anomalies With Regional P_W Variability[a]

	PC1	PC2	PC3
R1	−0.25 (66)	−0.14	0.06
R2	−0.06 (85)	0.07	0.15
R3	−0.25 (82)	−0.08	0.02
R4	**−0.32** (84)	**−0.71**	0.14
R5	**0.91** (71)	0.02	**0.44**
R6	**0.94** (66)	**0.45**	**0.28**
R7	**0.91** (65)	**0.29**	0.06

[a]Correlation coefficients, *r*, for mean winter principal components of basin-wide P_W anomalies (Figure 4) versus anomalous P_W PC1 over regions R1–R7 (see Figure 6). Correlations with *p* values ≤0.05 are in bold. Percent variance explained by mode 1 over respective regions is given in parentheses.

Upward trends during summer along the western boundary over R1 may be related to increasing hurricane intensity [*Bromirski and Kossin*, 2008], although this is not likely a factor in the Labrador Sea and near Nova Scotia.

The relationship between regional and basin-wide P_W variability was further investigated with correlations between regional average series and the basin-wide principal components (PCs) shown in Figure 2. Basin P_W PC1 is dominated by wave activity in the northeast Atlantic (Figures 2a and 2d) strongly influenced by the NAO ($r = 0.64$, Table 1). A separate set of PCs was constructed for the P_W anomalies in each of the seven regions shown in Figure 6a, with PC1 representing the dominant wave variability across each region. The percent of the variance captured by the first EOF mode for each of the regions varies with the size of the region (Table 2), with mode 1 explaining at least two thirds of the variance in each regions. The poor correlation between basin PCs and PC1 over regions R1–R3 in the western North Atlantic indicates that P_W variability in those regions is not closely associated with northeast Atlantic wave variability, and suggests that different atmospheric patterns are influencing wave activity in R1–R3 as opposed to R5–R7. The good correlation of R5–R7 PC1 with basin PCs reflects the strong influence of the NAO on *Pw* variability in those regions.

7.2. Association Between Regional P_W and Climate Patterns

For storm impacts preparedness, it is useful for coastal managers to be able to anticipate winter wave power intensity levels, given that regional P_W variability may be related to particular patterns of climate variability. Pronounced seasonal differences in synoptic variability across the North Atlantic makes seasonal correlations more useful than full-year comparisons to elucidate how winter coastal P_W intensity is associated with broad-scale variability. Relationships of P_W with climate variability were investigated by correlation of winter climate indices with winter (November–March) mode 1 principal components (PCs) for each of the regions shown in Figure 6a. The P_W data were normalized to unit variance prior to PC determination. Winter averages (November–March) of PCs and the climate indices were formed for use in the correlation analysis.

A differentiation of the dominant broad-scale climate patterns that affect wave activity over the North Atlantic is exhibited in Table 3, with North Pacific associations more influential on wave activity along the western boundary and North Atlantic atmospheric patterns dominating wave activity in the central and northeast Atlantic. Noteworthy is the weak association of P_W along the US. East Coast with NAO and AO, similar to that found by *Semedo et al*. [2011]. Correlations shown in Table 3 confirm that wave activity in regions R1–R3 is uncorrelated with North Atlantic climate variability characterized by NAO, consistent with r^2 values in Table 2. Correlations indicate that El Niño-Southern Oscillation (ENSO) variability, represented by NINO3.4, and the Pacific North America (PNA) patterns, both have a significant influence on P_W variability in the western North Atlantic.

Table 3. Correlation of Regional Mean Winter P_W Anomalies With Climate Indices[a]

	NAO	AMO	AO	NINO3.4	PDO	−NP	PNA
R1	−0.17 (66)	0.00	**−0.25**	**0.45**	**0.26**	**0.28**	**0.42**
R2	0.12 (85)	0.03	−0.09	**0.41**	**0.32**	0.23	**0.31**
R3	−0.14 (82)	0.00	−0.19	**0.42**	0.19	0.23	**0.38**
R4	**−0.59** (84)	0.10	**−0.56**	**0.30**	0.19	0.12	0.23
R5	**0.51** (71)	−0.20	**0.49**	0.08	0.17	−0.08	−0.09
R6	**0.80** (66)	**−0.26**	**0.73**	0.11	0.17	0.02	−0.03
R7	**0.72** (65)	**−0.26**	**0.59**	0.12	0.23	0.10	0.08

[a]Correlation coefficients, *r*, for principal component mode 1 (PC1) of mean winter (November–March) monthly P_W anomalies over regions R1–R7 shown in Figure 6. Average winter North Atlantic NAO, AMO, AO, and North Pacific NINO3.4, PDO, −NP, and PNA indices of climate variability. Correlations with *p* values ≤0.05 in bold. Percent variance explained by mode 1 over respective regions is given in parentheses under the NAO *r* values.

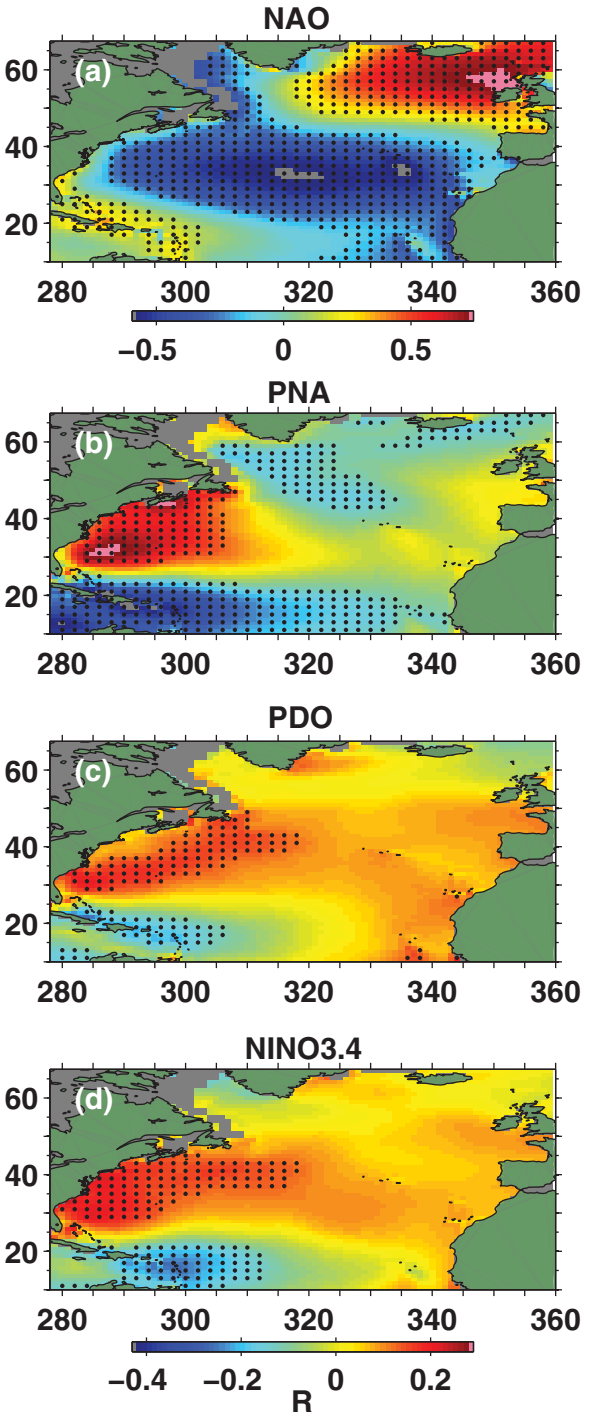

Figure 7. Correlation, *r*, between mean winter (November–March) wave power and indices of climate variability, with (b–d) showing North Pacific associations. Regions where *p* values $\leq$0.05 in at least 3 of 4 grid nodes over 2° × 2° boxes are indicated by dots. The strongest *Pw* climate associations are with NAO and AO (not shown), whose *r* levels and patterns are very similar, with the high *r* region off the British Isles for AO correlations displaced slightly northward of that shown for NAO. (d) *r* scale below also applies to Figures 7b and 7c.

Because the dominant region of winter North Atlantic P_W variation that encompasses R6 extends to Iceland (Figures 2a, 6a, and 6e), it is not surprising that NAO exhibits relatively strong correlations with the PC time series from regions R5–R7 (Table 3). Correlations in Table 3 also suggest that North Pacific climate variability has minimal correlation with wave activity in the northeast Atlantic on winter time scales. More central region R4 is negatively correlated with NAO and AO, consistent with EOF mode 1 and anomalous P_W patterns shown in Figures 2a and 6a. Correlations suggest that the Atlantic Multidecadal Oscillation (AMO) [*Enfield and Mestas-Nunez*, 1999] has less influence on winter activity over most of the North Atlantic.

The dominance of NAO on northeastern Atlantic winter P_W variability is emphasized by the relatively high correlations of P_W versus NAO shown in Figure 7a compared with correlations of P_W versus North Pacific climate indices shown in Figures 7b–7d. The NAO-P_W correlations show the characteristic NAO dipole pattern, with generally opposite phase and insignificant weak correlations along most of the U.S. East Coast, a similar but somewhat different pattern to that found in previous studies [e.g., *Semedo et al.*, 2011]. Although not strong, significant correlations of wave activity with PNA and NINO3.4 (Figures 7b and 7c) occur over the western North Atlantic, suggesting an association between North Pacific climate variability with winter P_W in this region.

7.3. Dominant North Atlantic Winter Wave Generation Locations

The portion of coasts most strongly impacted by intense wave activity is largely determined by the location of the dominant regional wave generation region. Identification of a systematic change in the location of dominant winter wave regions is key to explaining patterns of coastal impacts [*Bromirski et al.*, 2013], with their proximity and azimuth with respect to the Atlantic coasts of the United States and Europe and Iceland affecting both coastal wave amplitude and incident wave direction.

We expect the dominant wave generation region to be characterized by strong, repeated variation of *Hs* on synoptic time scales, whose dominant location can be identified using a within-winter EOF analysis of

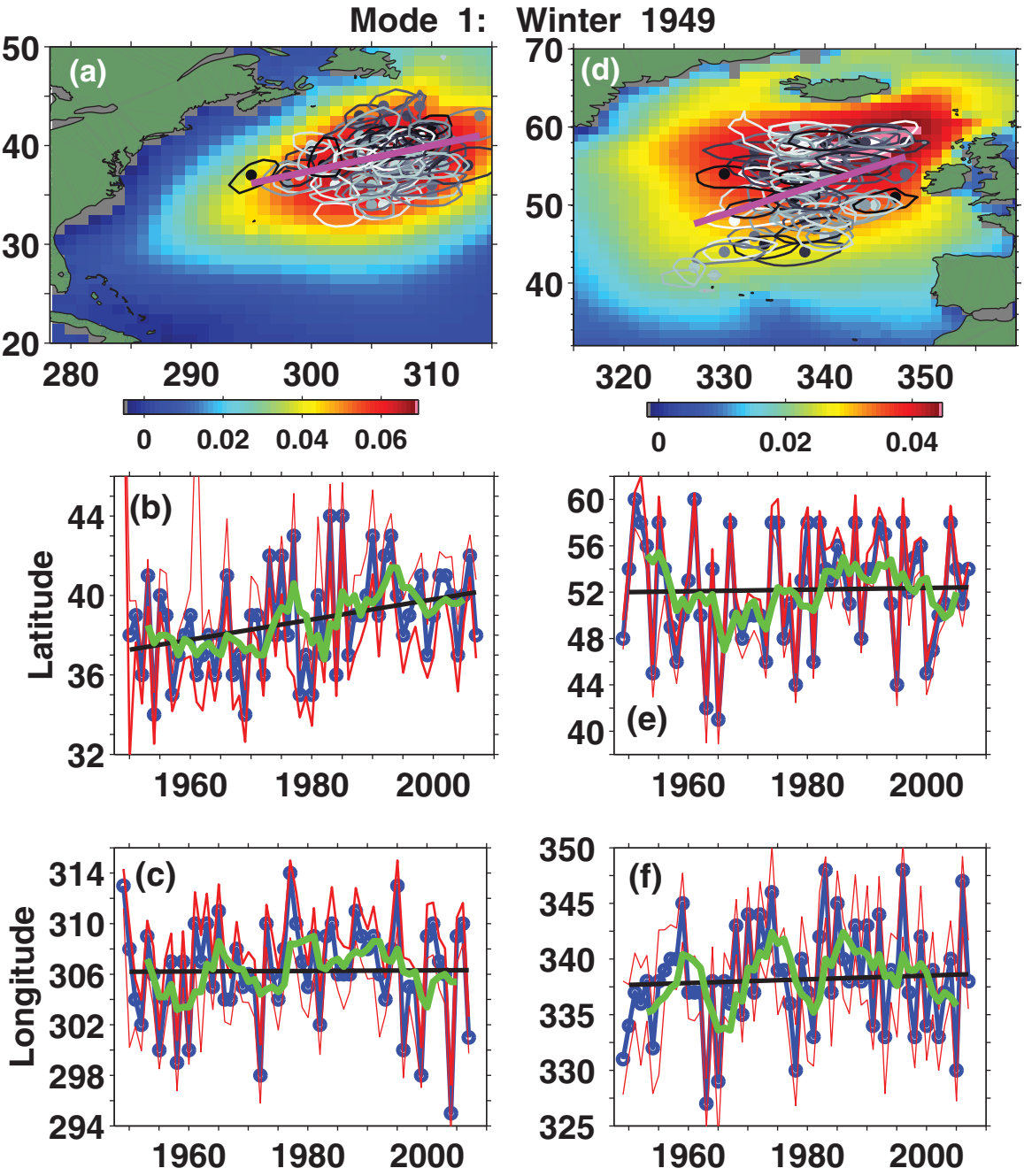

Figure 8. Year-to-year fluctuations in the dominant location of the greatest wave height variation over the (left) western and (right) northeastern North Atlantic during winter (November–March). Representative EOF spatial patterns of winter *Hs* over 1948–1949 in the (a) western and (d) northeastern North Atlantic. Successive winter peaks in mode 1 EOFs (dots) over these regions and their associated 98th percentile contours are color coded by year (light to dark). The least squares trend line of the longitudinally ordered EOF peaks (magenta line) gives an estimate of the central tendency of peak wave locations. (b, e) Latitude of the EOF peak (connected blue dots) and the range of their respective north-south 98th percentile extent (red lines), with the least squares trend (black line) and 5 year running mean (green line) also shown. (c, f) Same as Figures 8b and 8e except for longitude, with east-west extent shown instead. Only the least squares trend in Figure 8b is statistically significant.

synoptic variability. Thus, variability of the dominant wave generation region location in the western (20°N–50°N and 278°E–315°E) and eastern (32°N–70°N and 316°E–360°E) North Atlantic (Figures 8a and 8d, respectively) during winter (November–March) were investigated using a synoptic time scale wave height series, one set for each winter. This series was represented by EOFs calculated from the 6 h *Hs* fields. The spatial patterns in representative Figures 8a and 8d are color coded, from cool-to-warm, maps of weightings low-to-high, respectfully, of the mode 1 EOFs (computed over the 1948–1949 winter) of the 1949–2008 series.

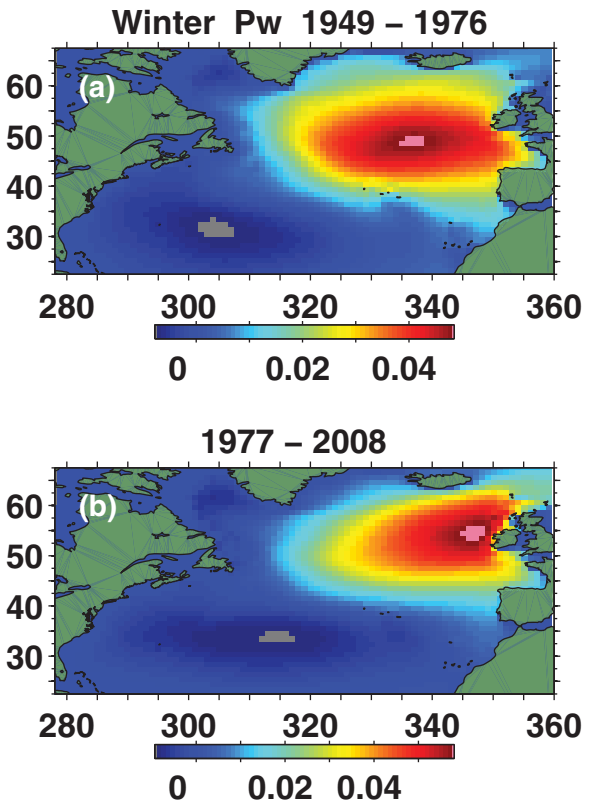

Figure 9. Empirical orthogonal function mode 1 of winter (e.g., November 1948 to March 1949 designated 1949) monthly wave power anomalies over the domain shown spanning the (a) 1948–1976 (modes 1, 2, 3; $\sigma^2 = 42, 26, 11$) and (b) 1977–2008 ($\sigma^2 = 42, 30, 9$) epochs. Modes 2 and 3 (not shown) have very similar patterns and dipole locations to those shown in Figures 5b and 5c over the two epochs, with a slight strengthening of the weightings along the western boundary for mode 2 during the latter epoch.

The sequence of locations of the peak of EOF 1 provides a measure of how the dominant winter *Hs* variability changes over the record. Winter *Hs* mode 1 typically accounts for about 37 and 32% of the *Hs* variance over the western and eastern regions, respectively.

7.3.1. Western North Atlantic Dominant Winter Waves

Substantial north-south and east-west excursions in the dominant North Atlantic wave generation region have occurred, as indicated by the location of greatest winter *Hs* synoptic scale variation over the western North Atlantic (Figures 8a–8c). Winters with westerly shifted centers of peak wave activity have greater impacts along the U.S. Atlantic coast. As a rule, the major pattern of synoptic time scale wave variability is concentrated north of 35°N and west of 310°E, although there are years when peak activity is shifted southward, e.g. occasional years from 1950 to 1980, with a general tendency for more northerly wave activity over the record length.

Latitude and longitude locations of the EOF mode 1 peaks (Figures 6c and 8b) show the north-south and east-west extents of dominant wave activity for each winter. Trend lines indicate any consistent shift in the mean latitude and longitude of peak wave activity that may have taken place over 1948–2008 time period. The spatial distribution of winter peak *Hs* locations (Figure 8a) is accompanied by a significant increase in latitude (northward trend) over the latter half of the twentieth century (Figure 8b, black line). Similar to the North Pacific [*Bromirski et al.*, 2013], there is considerable variability at time scales shorter than the long period trends, however. Since about 1995, winter 5 year running means (Figures 8b and 8c, green curves) show a tendency for a southwestward shift in the dominant centers of wave activity over the domain, i.e. closer to the coast. This apparent southwestward shift also appears to be consistent with an apparent intensification of the P_w mode 2 southern pole since 1977 (supporting information Figure S5).

7.3.2. Eastern North Atlantic Dominant Winter Waves

Similar to variability in the western North Atlantic, substantial north-south and east-west excursions of the location of peak winter *Hs* occur over the northeastern Atlantic (Figures 8d–8f). More southern excursions relative to the mean generally occur during the negative phase of the NAO. Latitude and longitude locations of peak winter *Hs* (Figures 8e and 8f, black lines) indicate no significant trends (the persistent recurrence of peak latitude at 58°N may be an artifact of the domain selected and/or the grid intervals), and represent the mean *Hs* peak position at about [52°N, 337.5°W], substantially different from the locations of winter peak *Pw* shown in Figures 1–4 and 6. However, the aforementioned figures included the epoch spanning the strongly positive phase of the NAO centered in the early 1990s (see Figure 10b), while in this analysis those years have equal weight and thus have less influence on the mean locations estimated.

Notable interdecadal variability is observed in the latitude and longitude of the dominant wave heights in the western and eastern North Atlantic (Figure 8e and 8f, green curves), with latitudes varying by five or more degrees and longitudes varying by 10 or more degrees. Of particular interest is the tendency for decreasing latitude and longitude since about 1990 when the long-term NAO was generally most positive (red curve,

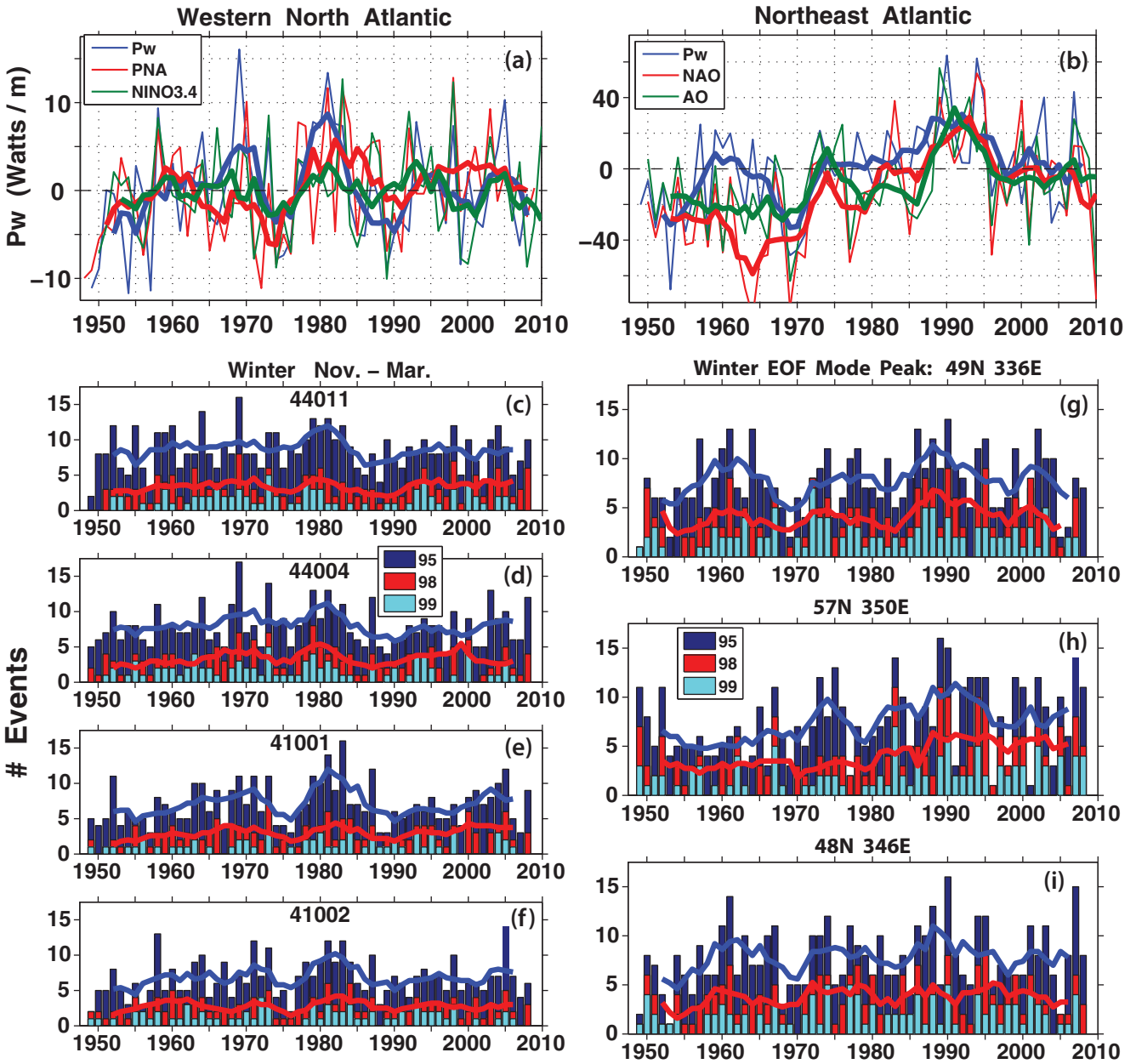

Figure 10. *Mean* anomalous winter (November–March) wave power, *Pw*, over (a) the western North Atlantic between 27°N and 47.5°N, extending the southeast corner of region 1 in Figure 6a to 295°E in order to encompass the high PNA correlation region in Figure 7b, and (b) over the northeast Atlantic between 37°N and 67.5°N and 315°E and 360°E (blue curves). Thick lines are associated 5 year running means depicting longer period variability. Also shown are corresponding scaled winter and 5 year patterns of the dominant modes of climate variability that influence Pw variability in these respective North Atlantic regions (see Tables 2 and 3 and Figure 7). (c–f) Number of extreme events with *Hs* exceeding the 95, 98, and 99 percentile *Hs* thresholds for at least 12 consecutive hours at offshore buoys (north to south) 44011, 44004, 41001, and 41002 during winter (see supporting information validation Figure V1 for buoy locations). (g–i) Same as Figures 10c–10f except at northeast Atlantic locations at the indicated winter EOF mode peak locations.

Figure 10b; green curve, Figure 11h), suggesting a general shift in the centers of peak *Hs* generation to the southwest as the NAO gradually shifted toward a stronger negative phase influence in the late 2000s.

8. Discussion

Changes in winter wave energy in specific regions of the North Atlantic, such as along the Atlantic coasts of North America and Europe, depend on the configuration of North Atlantic and upstream Pacific-North American atmospheric circulation patterns, including storm track and associated wind patterns and strength. The most important control on wave height and wave power is the NAO, which is associated with

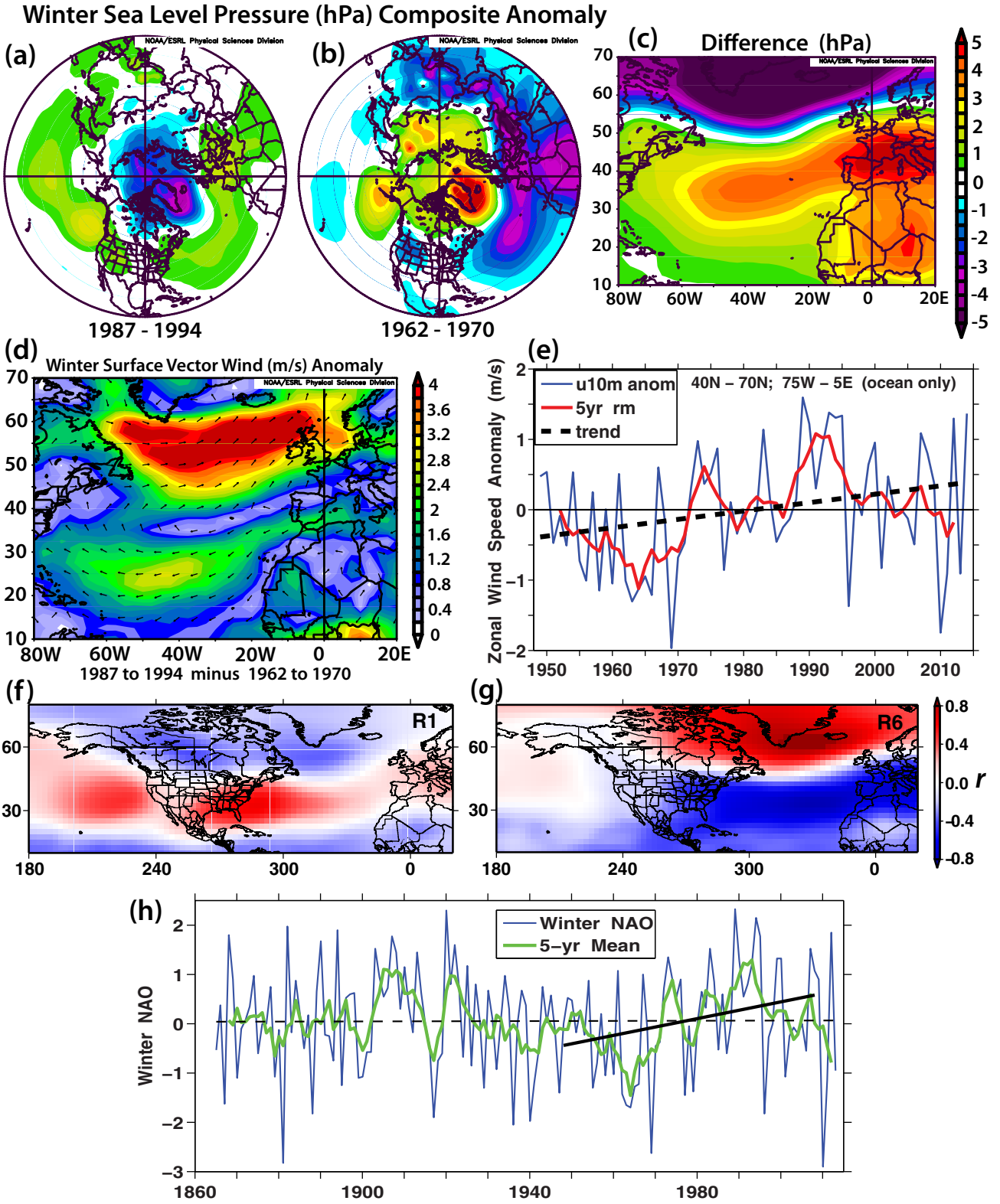

Figure 11. Sea level pressure composite anomalies (NCEP/NCAR Reanalysis 1) during winter (November–March) relative to the 1981–2010 climatology spanning predominantly (a) positive (1987–1994) and (b) negative (1962–1970) NAO winters. (c) Difference in sea level pressure (SLP) composite anomalies between those shown in Figures 11a and 11b, i.e., 1987–1994 minus 1962–1970. (d) Same as Figure 11c except for NCEP/NCAR Reanalysis 1 surface vector winds. (e) Winter mean zonal 10 m wind speed over the North Atlantic basin from 40°N to 70°N and 75°W to 5°E (blue) and the 5 year running mean (red), with the least squares fit (dashed) significantly different from zero at the 95% level. (f) Correlation between the mode 1 principal component (PC1) of anomalous P_W over western boundary region R1 (see Figure 6a) and 700 hPa height anomalies. (g) Same as Figure 11f except PC1 for northeastern Atlantic region R6. (h) Winter NAO spanning the 1865–2013 epoch (blue) with 5 year running mean (green). Least squares trend line over the entire record (dashed) is not significant, while the trend over the record of this study (1948–2008) is significant at the 95th percentile level.

monthly to interdecadal fluctuations in storm characteristics across the North Atlantic basin. The influence of the phase of the NAO on winter P_W distribution across the North Atlantic can be inferred from anomalous winter P_W EOF spatial patterns. To investigate NAO phase effects and possible associations with North Pacific variability, the monthly anomaly record was divided into two epochs as in *Bromirski et al.* [2013], with the early epoch primarily under negative NAO and the latter positive NAO (Figure 11h). The mode 1 EOF patterns for the two epochs in Figure 9 account for the same variance and show that the dominant pole during the positive phase (Figure 9b and supporting information Figure S5) is displaced about 10°E and 5°N relative to the negative phase, generally consistent with the northward shift in storm track found by *Wang et al.* [2006] over the 1958–2001 epoch. The principal high activity region is along the coast of Ireland, consistent with the location of steep trends in winter Pw_{90T} (Figure 4a) and winter P_E (Figure 5d). These results reflect the expectation that NAO is most pronounced during winter, with a northward shift in storm tracks associated with its strong positive phase from the early 1980s to mid-1990s [*Hurrell and van Loon*, 1997].

The controlling influence of NAO on winter P_W is also emphasized by lower wave heights and P_W during the post-2000 decline in the NAO; this followed a period in the late 1980s through early 1990s when P_W levels were predominantly high during the dominant positive NAO (Figures 6c and 10b). The influence of record length in conjunction with NAO decadal fluctuations on P_W trends is reflected in satellite altimetry-derived *Hs* trend estimates over the northeast Atlantic by *Young et al.* [2011], who found generally low-upward or downward trends over 1985–2008. The altimetry estimates are in contrast to strongly upward long-term trends determined here and by others from longer records. The trends determined by Young et al. are likely strongly influenced by the position of the satellite record with respect to NAO decadal variability, with higher waves at the beginning of that record when the NAO was strongly positive.

Basin-wide P_W levels during the post-2000 period (Figure 6c) are comparable to those prior to 1980, suggesting that observed trends and patterns are not affected by systematic biases in the NRA-1 forcing winds, but result from actual changes in atmospheric circulation associated with the phase of the NAO. These results reflect a shift in storm track to the south and west resulting from NAO-related atmospheric decadal variability during the negative phase of the NAO, and to the northeast during positive NAO.

Identifying the influence of predominant broad-scale climate patterns on heightened wave activity is useful for winter coastal planning preparedness. The western and northeastern North Atlantic are subject to different climate controls, determined from P_W correlations with climate indices (Figure 7 and Tables 1 and 3). Inspection of winter mean P_W over these regions (Figures 10a and 10b) confirms that they are uncorrelated, emphasized by the minimum in long-term variability near 1990 in Figure 10a, as opposed to the maximum in Figure 10b at that time (thick blue lines). Comparison of the long-term variability of PNA and NINO3.4 indices with mean winter P_W in Figure 10a indicates that heightened (reduced) wave activity is more common when PNA and NINO3.4 (a proxy for El Niño) are positive (negative) and in phase. Similarly, when NAO and AO are in phase (Figure 10b), heightened wave activity is more common when both are strongly positive. P_W relationships between Figures 10a and 10b are consistent with the assessment that PNA teleconnections occur in opposition to changes associated with the NAO [*Hurrell and van Loon*, 1997].

The frequency of strong events along coasts is also important to coastal managers for response planning and preparedness. The number of events in each winter was determined in the western (at selected NOAA buoy locations) and northeastern Atlantic (at the location of EOF peaks) for *Hs* thresholds at each location determined by respective 95th, 98th, and 99th *Hs* percentile levels using the same methodology as in Figure 5. As might be expected, the variability of the number of winter events track mean winter P_W (compare thick lines for the western and northeast Atlantic), with elevated event counts more common during peak P_W winters. Notably, about a 25% increase in strong events compared with average winters occurs during winters with heightened mean P_W in the northwestern Atlantic identified in Figure 10a. Similarly, during extreme positive NAO winters in the northeastern Atlantic (represented by Figure 10h), the number of strong events exceeds the mean occurrences by at least 50%. Note that the P_W location in Figure 10g near 49°N 336°E is close to that for the basin-wide EOF in Figure 9a, that Figure 10h primarily represents conditions under strongly positive NAO during the early 1990s (as in Figure 9b), and that Figure 10i represents the EOF mode 3 pole Bay of Biscay activity in Figure 2c (and supporting information Figure S5). The generally increased occurrence of strong events since about 1985 along the Irish coast (Figure 10h) is likely associated with the northeastward shift in the dominant P_w mode 1 EOF peak during the second half of the analysis period (compare Figures 9a and 9b).

The hindcast indicates that the northeastern Atlantic wave height and wave power, P_W, have considerable variability that is associated with the NAO over monthly to interdecadal time scales. Links of the NAO with hindcast seasonal wave power variability and associated storm activity are supported by comparison of SLP and near surface wind across the North Atlantic (Figure 11) during the positive (1987–1994) and negative (1962–1970) phases of winter NAO. The November-through-March SLP composite during positive NAO winters (Figures 11a and 11h) shows a deepened Icelandic low, whose negative anomalies and strong gradient indicate more intense storm activity over the North Atlantic. In contrast, the winter SLP composite associated with negative-NAO winters (Figure 11b) shows positive anomalies over Iceland and Greenland, with negative anomalies to the south, effectively displacing the Icelandic low southeastward. Figures 11a and 11b reflect the anomalous P_w patterns shown in Figure 9.

The difference between the contrasting NAO winter SLP patterns (Figure 11c) results in a strong SLP gradient that would produce strong winds over the North Atlantic. The difference in near surface wind between the same composite NAO winters (Figure 11d) exhibits the strongest wind difference over the North Atlantic north of 45°N directed toward the region in the northeastern Atlantic where the greatest upward P_E trends are observed (Figures 5a and 5d). Consistent with this intensification is the upward trend in winter zonal wind anomalies across the North Atlantic over 40°N–70°N and 75°W–5°E (Figure 11e). The association of the strengthened NAO with heightened winds across the higher mid-latitudes of the North Atlantic is particularly evident during the late 1980s to mid-1990s under strongly positive NAO. Conversely, subdued winds occurred during the dominant negative phase prior to 1970. The result of these anomalous NAO episodes is an upward trend in P_E off the coasts of Ireland and Scotland, as can be seen in Figures 5a and 5d. It is interesting that recent positive anomalous zonal wind speed excursions since 2010 in Figure 11e have reached levels not seen since the early 1990s. The deep negative zonal wind anomaly during 2010 is comparable to levels during the strongly negative NAO phase prior to 1970, suggesting that changes in observations and observation practices, such as the advent of remote-sensed information that were introduced in the Global Reanalysis in the late 1970s, have not introduced a significant upward bias in the surface wind field.

The influence of broad-scale atmospheric patterns on North Atlantic anomalous regional P_W is further demonstrated by correlations of regional P_W with 700 hPa height anomalies. The correlation pattern of anomalous P_W mode 1 principal component (PC1) in region R1 (see Figure 6a) with 700 hPa height anomalies (Figure 11f) resembles the PNA, with strong similarity to the PNA correlation pattern with mean winter P_W over the western North Atlantic (Figure 7b). Correlations with northeastern Atlantic region R6 PC1 produces a pattern that is consistent with the dominant NAO influence on winter P_W shown in Figure 7a. The SLP and associated surface wind anomalies and correlation patterns shown in Figure 11 are consistent with the NAO correlations in Tables (1–3), and emphasize heightened (subdued) wave activity during the positive (negative) phase of the NAO that has a strong influence on the northeastern Atlantic long-term trends.

The upward trend in NAO since 1948 contrasts with the lack of a significant winter NAO trend over the 1865–2013 epoch (shown in Figure 11h, dashed line), suggesting that the long-term upward trend in wave activity over the northeast Atlantic since 1950 resulting from the recent strongly positive NAO in the early 1990s may not persist. Note that steeper upward trends in NAO, and therefore wave energy, would result from records beginning closer to the NAO minimum near 1960 and/or ending nearer the NAO maximum in the early 1990s.

Interestingly, although it was not included in the wave model simulation, the 2013–2014 winter exhibited periods when the NAO reverted to its positive phase (http://www.cpc.ncep.noaa.gov/products/precip/CWlink/pna/nao_index.html), evidenced by catastrophic flooding in England during February 2014. This heightened storm activity underscores the importance fluctuations of atmospheric circulation in the North Atlantic basin, demonstrating that there are strong fluctuations on interannual time scales, and that decadal spells do not necessarily indicate secular changes.

9. Summary and Conclusions

Analysis of a WW3 hindcast (1948–2008) provides a better understanding of North Atlantic wave height, wave power variability, and estimates of their underlying trends. Open ocean wave variability has good fidelity with western North Atlantic open ocean buoy records, and to some extent with coastal buoy records. Furthermore, wave variability is reasonably consistent in its relationship to large-scale climate

measures during the period before and after the peak in the strongly positive NAO that occurred during the mid-1980s to mid-1990s. To better understand wave characteristics and their potential impacts, this study not only investigates significant wave height, *Hs*, but also wave power, P_W, which increases nonlinearly with *Hs* and is proportional to *Tp*.

The hindcast exhibits a general increase in winter *Hs* and *Pw* over most of the northeast Atlantic since 1950. In that region, fluctuations in winter wave *Hs*, *Pw*, and seasonal aggregates of high wave events have a relatively strong connection to the NAO and AO. Increases in wave intensity in the northeast Atlantic were found when both NAO and AO were positive. Averaged over the North Atlantic (north of 15°N), mean winter wave power, compared with mean pre-1975 levels, increased by about 15% during the NAO positive phase from about 1985–1995, with peak winter wave levels about 30% greater. The placement in time of these NAO-related fluctuations has a strong influence on the upward trends that have resulted (Figure 11h, thick black), which reflect the influence of the combination of predominantly strongly negative NAO spanning about 1950–1970 followed by the strongly positive NAO during the 1980s and 1990s (Figure 11h, green curve).

Upward trends in the *number* of strong wave power events (P_E) during winter (November–March) are confined primarily to northeastern Atlantic, with changes exceeding one event per year per decade. The pattern of change in strong event *magnitude* spans a similar region, with steepest winter P_E increases in a region close to the Atlantic coasts of the British Isles and Iceland, in consort with increases in Hs_{90} or Pw_{90}. The duration of strong P_E events has generally not increased over the North Atlantic. In summer, increased numbers of events occur more prevalently in the western North Atlantic. The strongest upward trends in summer event magnitude occur in the Bay of Biscay and along the Icelandic coast. However, over much of the North Atlantic, summer wave power trends do not follow the pattern of increases seen in winter, reflecting a reduced influence of NAO in summer.

Although the overall 1948–2008 record exhibits upward trends in P_w over the North Atlantic basin, since about 2000 there has been a reversal. This reversal is similar to a shift toward reduced wave activity over the North Pacific since 1999, which has been predominantly affected by the PDO cool phase. The recent decline in North Atlantic basin-wide P_w levels is consistent with lower wave activity during the negative phase of NAO, which has become more prevalent during this recent period (Figure 11h, green curve). If the negative NAO persists, wave activity will probably remain subdued which would reduce or eventually negate the upward trends in the northeastern Atlantic seen over 1948–2008. The magnitude and sign of the trends described are highly influenced by the timing of particular patterns of interannual and longer-term decadal NAO fluctuations [*Hurrell et al*., 2003], i.e., by strongly positive NAO during the mid-1980s to mid-1990s when the NAO was its strongest since the 1860s [*Hurrell*, 1995]. This period strongly influences the strong upward trends over the northeastern Atlantic observed by this and other studies over the latter half of the twentieth century.

These results for the North Atlantic have some interesting similarities found in a recent study of wave fluctuations in the North Pacific over the same time period by *Bromirski et al*. [2013]. Both basins show increasing regional trends, but both are strongly affected by fluctuating modes of climate variability, dominated by the NAO in the North Atlantic and the PDO plus the El Niño/Southern Oscillation in the North Pacific. The present study reinforces the conclusion that natural climate modes, in this case the NAO, exert strong control in driving multidecade trends.

It is emphasized that trends over 1948–2008 should not be considered to be a prediction of future changes, because of the strong control imposed by climate patterns whose fluctuations (presumably resulting from natural variability) will likely continue. Regardless of the cause of the P_w trends, the northeastern Atlantic coastal regions are more exposed to impacts from wave-generated erosion and flooding. Coastal impacts under any climate regime will be accentuated when high waves occur near peak high tides, and will be exacerbated as sea level continues to rise.

Acknowledgments

Support for this study is gratefully acknowledged from NOAA through grant NA10OAR4310121 and the California Department of Parks and Recreation, Division of Boating and Waterways under contract 11–106-107 with SIO, as is support for D.R.C. from the NOAA RISA program. We thank Paul Wittmann and John Helly (hellyj@ucsd.edu) for providing the wave model data used in this study, archived at the San Diego Supercomputer Center, and Karen Barfoot at the UK Met Office (http://www.metoffice.gov.uk) for providing archived buoy data from the northeast Atlantic and NOAA NODC (http://www.nodc.noaa.gov) for buoy data from the western North Atlantic.

References

Bacon, S., and D. J. T. Carter (1991), Wave climate changes in the North Atlantic and North Sea, *Int. J. Climatol.*, *11*, 545–558.

Bacon, S., and D. J. T. Carter (1993), A connection between mean wave height and atmospheric pressure gradient in the North Atlantic, *Int. J. Climatol.*, *13*, 423–436.

Barnston, A. G., and R. E. Livezey (1987), Classification, seasonality, and persistence of low-frequency atmospheric circulation patterns, *Mon. Weather Rev.*, *115*, 1825–1850.

Bidlot, J.-R., D. J. Holmes, P. A. Wittmann, R. Lalbeharry, and H. S. Chen (2002), Intercomparison of the performance of operational ocean wave forecasting systems with buoy data, *Weather Forecasting*, *17*, 287–310.

Bouws, E., D. Jannink, and G. J. Komen (1996), The increasing wave height in the North Atlantic Ocean, *Bull. Am. Meteorol. Soc.*, *77*, 2275–2277.
Bromirski, P. D., and R. E. Flick (2008), Storm surge in the San Francisco Bay/Delta and nearby coastal locations, *Shore Beach*, *76*(3), 29–37.
Bromirski, P. D., and J. P. Kossin (2008), Increasing hurricane wave power along the U.S. Atlantic and Gulf Coasts, *J. Geophys. Res.*, *113*, C07012, doi:10.1029/2007JC004706.
Bromirski, P. D., D. R. Cayan, J. Helly, and P. Wittmann (2013), Wave power variability and trends across the North Pacific, *J. Geophys. Res. Oceans*, *118*, 6329–6348, doi:10.1002/2013JC009189.
Caires, S., A. Sterl, J.-R. Bidlot, N. Graham, and V. Swail (2004), Intercomparison of different wind-wave reanalyses, *J. Clim.*, *17*(10), 1893–1913.
Carter, D. J. T., and L. Draper (1988), Has the northeast Atlantic become rougher?, *Nature*, *332*, 494.
Cassou, C., L. Terray, J. W. Hurrell, and C. Deser (2004), North Atlantic winter climate regimes: Spatial asymmetry, stationarity with time, and oceanic forcing, *J. Clim.*, *17*, 1055–1068.
Cayan, D. R., P. D. Bromirski, K. Hayhoe, M. Tyree, M. D. Dettinger, and R. E. Flick (2008), Climate change projections of sea level extremes along the California coast, *Clim. Change*, *87*, 57–73, doi:10.1007/s10584-007-9376-7.
Chang, E. K. M. (2007), Assessing the increasing trend in Northern Hemisphere winter storm track activity using surface ship observations and a statistical storm track model, *J. Clim.*, *20*, 5607–5628.
Charles, E., D. Idier, J. Thiebot, G. Le Cozannet, and R. Pedreros (2012), Present wave climate of the Bay of Biscay: Spatiotemporal variability and trends from 1958 to 2001, *J. Clim.*, *25*, 2020–2039.
Clément, A., et al. (2002), Wave energy in Europe: Current status and perspectives, *Renewable Sustainable Energy Rev.*, *6*(5), 405–431, doi: 10.1016/S1364-0321(02)00009-6.
Cox, A. T., and V. R. Swail (2001), A global wave hindcast over the period 1958–1997: Validation and climate assessment, *J. Geophys. Res.*, *106*(C2), 2313–2329.
Davis, R. E., R. Dolan, and G. Demme (1993), Synoptic climatology of Atlantic coast north-easters, *Int. J. Climatol.*, *13*(2), 171–189.
Deser, C. (2000), On the teleconnectivity of the Arctic Oscillation, *Geophys. Res. Lett.*, *27*(6), 779–782.
Dodet, G., X. Bertin, and R. Taborda (2010), Wave climate variability in the North-East Atlantic Ocean over the last six decades, *Ocean Modell.*, *31*, 120–131.
Dolan, R., and R. E. Davis (1992), An intensity scale for Atlantic coast northeast storms, *J. Coastal Res.*, *8*(4), 840–853.
Dolan, R., H. Lins, and B. Hayden (1988), Mid-Atlantic coastal storms, *J. Coastal Res.*, *4*(3), 417–433.
Enfield, D. B., and A. M. Mestas-Nunez (1999), *J. Clim.*, *12*, 2719–2733.
Franzke, C., S. Lee, and S. B. Feldstein (2004), Is the North Atlantic oscillation a breaking wave?, *J. Atmos. Sci.*, *61*, 145–160.
Gemmrich, J., B. Thomas, and R. Bouchard (2011), Observational changes and trends in northeast Pacific wave records, *Geophys. Res. Lett.*, *38*, L22601, doi:10.1029/2011GL049518.
Geng, Q., and M. Sugi (2001), Variability of the North Atlantic cyclone activity in winter analyzed from NCEP-NCAR reanalysis data, *J. Clim.*, *14*, 3863–3873.
Graham, N. E., and H. F. Diaz (2001), Evidence for intensification of North Pacific winter cyclones since 1948, *Bull. Am. Meteorol. Soc.*, *82*(9), 1869–1893.
Hines, W. H., and D. C. Montgomery (1980), *Probability and Statistics in Engineering and Management Science*, 634 pp., John Wiley, New York.
Hirsch, M. E., A. T. DeGaetano, and S. J. Colucci (2001), An East Coast winter storm climatology, *J. Clim.*, *14*(5), 882–899.
Honda, M., and H. Nakamura (2001), Interannual seesaw between the Aleutian and Icelandic Lows. Part II: Its significance in interannual variability over the wintertime Northern Hemisphere, *J. Clim.*, *14*, 4512–4529.
Hoskins, B. J., and K. I. Hodges (2002), New perspectives on the Northern Hemisphere winter storm tracks, *J. Atmos. Sci.*, *59*, 1041–1061.
Hurrell, J. W. (1995), Decadal trends in the North Atlantic oscillation regional temperatures and precipitation, *Science*, *269*, 676–679.
Hurrell, J. W., and H. van Loon (1997), Decadal variations in climate associated with the North Atlantic oscillation, *Clim. Change*, *36*, 301–326.
Hurrell, J. W., Y. Kushnir, G. Ottersen, and M. Visbeck (2003), An overview of the North Atlantic Oscillation, in *The North Atlantic Oscillation: Climatic Significance and Environmental Impact*, edited by J. W. Hurrell et al., 279 pp., AGU, Washington, D. C., doi:10.1029/134GM01.
IPCC (2013), *Climate Change 2013: The Physical Science Basis. Contribution of Working Group I to the Fifth Assessment Report of the Intergovernmental Panel on Climate Change*, edited by T. F. Stocker et al., 1535 pp., Cambridge Univ. Press, Cambridge, U. K., doi:10.1017/CBO9781107415324.
Kalnay, E., et al. (1996), The NCEP/NCAR 40-year reanalysis project, *Bull. Am. Meteorol. Soc.*, *77*, 437–471.
Kinsman, B. (1965), *Wind Waves: Their Generation and Propagation on the Ocean Surface*, 676 pp., Prentice Hall, Englewood Cliffs, N. J.
Kumar, A., and M. P. Hoerling (2003), The nature and cause for the delayed atmospheric response to El Niño, *J. Clim.*, *16*, 1391–1403.
Kushnir, Y., V. J. Cardone, J. G. Greenwood, and M. A. Cane (1997), The increase in North Atlantic wave heights, *J. Clim.*, *10*, 2107–2113.
Mantua, N. J., S. R. Hare, Y. Zhang, J. M. Wallace, and R. C. Francis (1997), A Pacific interdecadal climate oscillation with impact on salmon production, *Bull. Am. Meteorol. Soc.*, *78*, 1069–1079.
Mather, J. R., H. Adams III, and G. A. Yoskioka (1964), Coastal storms of the eastern United States, *J. Appl. Meteorol.*, *3*, 693–706.
Mather, J. R., R. T. Field, and G. A. Yoskioka (1967), Storm hazard damage along the East Coast of the U.S., *J. Appl. Meteorol.*, *6*, 20–30.
McCabe, G. J., M. P. Clark, and M. C. Serreze (2001), Trends in northern hemisphere surface cyclone frequency and intensity, *J. Clim.*, *14*, 2763–2768.
Semedo, A., K. Sušelj, A. Rutgersson, and A. Sterl (2011), A global view on the wind sea and swell climate and variability from ERA-40, *J. Clim.*, *24*, 1461–1479, doi:10.1175/2010JCLI3718.1.
Sterl, A. (2004), On the (in)homogeneity of reanalysis products, *J. Clim.*, *17*, 3866–3873.
Stockdon, H. F., R. A. Holman, P. A. Howd, and A. H. Sallenger (2006), Empirical parameterization of setup, swash, and runup, *Coastal Eng.*, *53*, 573–588.
Swail, V. R., and A. T. Cox (2000), On the use of NCEP-NCAR reanalysis surface marine wind fields for a long-term North Atlantic wave hindcast, *J. Atmos. Oceanic Technol.*, *17*, 532–545.
Thompson, D. W. J., and J. M. Wallace (1998), The Arctic Oscillation signature in the wintertime geopotential height and temperature fields, *Geophys. Res. Lett.*, *25*(9), 1297–1300.
Thompson, D. W. J., and J. M. Wallace (2000), Annular modes in the extratropical circulation. Part I: Month-to-Month variability, *J. Clim.*, *13*, 1000–1016.
Tolman, H. L. (2006), Toward the third release of WAVEWATCH III: A multi-grid model version, in *Proceedings of 9th International Workshop on Wave Hindcasting and Forecasting*, 12 pp., Victoria, Canada.

Tolman, H. L. (2009), *User Manual and System Documentation of WAVEWATCH III, Version 3.14*, U.S. Dep. of Commerce, NOAA, NWS, NCEP, Ocean Model. Branch, Camp Springs, Md.
Trenberth, K. E., and J. W. Hurrell (1994), Decadal atmosphere-ocean variations in the Pacific, *Clim. Dyn.*, *9*, 303–319.
Wallace, J. M., and D. S. Gutzler (1981), Teleconnections in the geopotential height field during the Northern Hemisphere winter, *Mon. Weather Rev.*, *109*, 784–812.
Wang, X. L., and V. R. Swail (2001), Changes of extreme wave heights in northern hemisphere oceans and related atmospheric circulation regimes, *J. Clim.*, *14*, 2204–2221.
Wang, X. L., V. R. Swail, and F. W. Zwiers (2006), Climatology and changes of extra-tropical cyclone activity: Comparison of ERA-40 with NCEP/NCAR reanalysis for 1958–2001, *J. Clim.*, *19*, 896–915, doi:10.1175/JCLI3781.1.
Wang, X. L., F. W. Zwiers, V. R. Swail, and Y. Feng (2008), Trends and variability of storminess in the Northeast Atlantic region, *Clim. Dyn.*, *33*, 1179–1195, doi:10.1007/s00382-008-0504-5.
Wang, X. L., V. R. Swail, F. W. Zwiers, X. Zhang, and Y. Feng (2009), Detection of external influence on trends of atmospheric storminess and ocean wave heights, *Clim. Dyn.*, *32*, 189–203, doi:10.1007/s00382-008-0442-2.
WASA Group (1995), The WASA project: Changing storm and wave climate in the Northeast Atlantic and adjacent seas?, in *Proceedings of Fourth International Workshop on Wave Hindcasting and Forecasting*, pp. 31–44, Environ. Canada, Banff, Alberta, Canada.
Wettstein, J. J., and J. M. Wallace (2010), Observed patterns of month-to-month storm-track variability and their relationship to background flow, *J. Atmos. Sci.*, *67*, 1420–1437.
Woolf, D. K., P. G. Challenor, and P. D. Cotton (2002), Variability and predictability of North Atlantic wave climate, *J. Geophys. Res.*, *107*(10), 3135, doi:10.1029/200/2001JC001124.
Young, I. R., S. Zieger, and A. V. Babanin (2011), Global trends in wind speed and wave height, *Science*, *332*, 451–455, doi:10.1126/science.1197219.